Evolving black holes from conformal transformations of static solutions

Marina M. C. Mello, Alan Maciel, and Vilson T. Zanchin

Centro de Ciências Naturais e Humanas, Universidade Federal do ABC, Avenida dos Estados 5001,
09210-580 Santo André, São Paulo, Brazil

A class of nonstationary spacetimes is obtained by means of a conformal transformation of the Schwarzschild metric, where the conformal factor $a(t)$ is an arbitrary function of the time coordinate only. We investigate several situations including some where the final state is a central object with constant mass. The metric is such that there is an initial big-bang type singularity and the final state depends on the chosen conformal factor. The Misner-Sharp mass is computed and a localized central object may be identified. The trapping horizons, geodesic and causal structure of the resulting spacetimes are investigated in detail. When $a(t)$ asymptotes to a constant in a short enough time scale, the spacetime presents an event horizon and its analytical extension reveals black-hole or white-hole regions. On the other hand, when $a(t)$ is unbounded from above as in cosmological models, the spacetime presents no event horizons and may present null singularities in the future. The energy-momentum content and other properties of the respective spacetimes are also investigated.

I. INTRODUCTION

The exact solutions of general relativity (GR) mostly used to model realistic objects in astrophysics and in cosmology may roughly be divided into two classes: static/stationary vacuum solutions that model the gravitational field outside massive objects or black holes, and homogeneous expanding solutions that are used as models for the large scale structure of the Universe. The first class aims to describe localized objects while the second one describes the global scale of the Universe. The fact that both class of solutions are successful in so different scales highlights that those scales are physically disconnected from each other. The interest in joining in one single picture these two aspects of gravitational physics is long standing, as is the question of how bound gravitational systems are insensitive to the cosmological expansion in large scale. These issues can be traced to the McVittie proposal of a metric describing a point mass in an expanding universe in 1933 [1], the Einstein-Strauss model [2] and the Lemaitre-Tolman-Bondi models [3,4]. These works founded the three main approaches to this issue, respectively, the crafting of analytical solutions with the wished asymptotics, the matching between the two types of solution, and the analysis of Einstein dynamical equations for some specified fluid content.

The matching approach has led to the Swiss-cheese models, that allow us to describe an expanding inhomogeneous universe filled with static bubbles that behave as if they were shielded from each other. Those models are interesting in order to study physics in an inhomogeneous universe [5,6] but they are too rigid to be considered the solution for the linking of local and global scales, because they rely strongly on the isotropy of the expansion and the spherical symmetry of the matching [7,8].

The dynamical analysis approach is the one that allows for the most realistic description of the transient regime between local and global scales, since a realistic fluid can be chosen as the source of the geometry, and the dynamical equations give the complete evolution of all physical quantities. However, the complexity of Einstein field equations is a formidable obstacle for the achievement of a general understanding of the transition between the global scale and the local scale behavior. With the simplifying assumption of spherical symmetry, some advance had been made, namely, the definition of a dynamically motivated separating surface between the two regimes, named matter trapping shells in the series of papers [9–13].

In the present paper we follow the McVittie lineage. Namely, we study the properties of a class of solutions proposed by Thakurta [14] as a model of cosmological black-hole spacetime, which are obtained by multiplying the Kerr solution by an expanding scale factor $a(t)$. However, the experience with the McVittie solution shows that identifying the content of a line element is not a simple task and the understanding of the causal structure of McVittie spacetimes had to wait about 80 years to be achieved since its publication [15–21]. Moreover, the McVittie metric was found to be richer than the original intent, with the possibility of representing black holes and/or white holes immersed in an expanding universe. A possible explanation for such a lapse of time may be the little interest in the McVittie metric, but it may also be attributed to the lack of mathematical tools available for studying dynamical spacetimes. However, in the last two decades there was a great development in this field (see, e.g., [22–27] and references there in), which has allowed for a systematical approach in order to understand dynamical solutions of GR, including cosmological black holes.

In this paper we make use of these tools in order to study thoroughly the nonrotating Thakurta solution, identifying all its possible outcomes with the main objective of finding examples of cosmological black holes. As the McVittie solution, the Thakurta solution can show a wide range of different properties, depending on the choice of the scale factor $a(t)$. For increasing and unbounded $a(t)$, as in cosmological models, we show that the Thakurta spacetime does not describe a cosmological black hole but rather an inhomogeneous expanding universe that may be either future geodesically complete or may present a future null singularity depending on the behavior of $a(t)$ for large times. On the other hand, for bounded $a(t)$, we establish sufficient conditions on $a(t)$ under which the Thakurta metric does present an event horizon at $r = 2m$. Moreover, we show that such an event horizon can be a black-hole horizon or a white-hole horizon depending on a further condition on $a(t)$.

This paper is organized as follows. In Sec. II we review the general properties of the Thakurta metric, analyze its source and the Misner-Sharp mass. In Sec. III we study the loci of coordinate and curvature singularities, the behavior of the trapping horizons and its dependency on the choice of $a(t)$, future and past geodesic completeness. Section IV contains the properties of the locus given by $r = 2m$ and study the conditions on $a(t)$ that implies that this surface can either be a future null singularity or a traversable horizon, using this result to build cosmological black-hole models. In Sec. V we analyze thoroughly the possible types of conformal diagrams corresponding to different choices of $a(t)$, including the possible analytical extensions when the $r = 2m$ surface is traversable, and discuss the physical content of each kind of solution. In Sec. VI we make further comments and conclude.

Throughout the paper, derivatives with respect to the t coordinate are denoted with an overhead dot. We use signature $(-, +, +, +)$ and natural units with $G = 1 = c$.

II. THE THAKURTA METRIC

A. Overview

The proposal of this paper is to study the nonrotating class of solutions emerging from the metric presented by Thakurta in 1981 [14]. The metric originally was built as a conformal transformation of Kerr rotating black-hole solution, whose conformal factor depends only on the Boyer-Lindquist time coordinate. The Thakurta metric is given by

$$ds^2 = a^2(\eta)\left[-\frac{\Delta}{\Sigma^2}(d\eta - j\sin^2\theta d\phi)^2 + \frac{\Sigma^2 dr^2}{\Delta} + \Sigma^2 d\theta^2 \right.$$
$$\left. + \frac{\sin^2\theta}{\Sigma^2}[(r^2 + j^2)d\phi - j\sin^2\theta d\eta]^2\right],\qquad(1)$$

with $\Sigma = r^2 + j^2\cos^2\theta$ and $\Delta = r^2 + j^2 - 2mr$, where m and j are constant parameters. In the case $a(\eta) = $ constant

metric Eq. (1) reduces to the Kerr metric, with m and j being respectively the mass and the angular momentum per unit mass of the Kerr black-hole metric. On the other hand, for large r the Thakurta metric asymptotes to the flat Friedmann-Lemaître-Robertson-Walker (FLRW) cosmological metric. Hence, the coordinate η and the function $a(\eta)$ are respectively the conformal time and the scale factor of the asymptotic FLRW metric.

Our proposal is to analyze the nonrotating Thakurta metric, that is, we set the angular momentum j to zero, so that the metric assumes the form

$$ds^2 = a^2(\eta)\left[-\left(1 - \frac{2m}{r}\right)d\eta^2 + \frac{dr^2}{1 - \frac{2m}{r}} + r^2 d\Omega^2\right]$$
$$= -\left(1 - \frac{2m}{r}\right)dt^2 + \frac{a^2(t)dr^2}{1 - \frac{2m}{r}} + a^2(t)r^2 d\Omega^2,\qquad(2)$$

where the cosmological time t, defined by $dt = a(\eta)d\eta$, was introduced.

It is worth to write here the Thakurta metric in terms of the areal radius coordinate $R = a(t)r$,

$$ds^2 = -\left(1 - \frac{2M(t)}{R} - \frac{H^2(t)R^2}{1 - \frac{2M(t)}{R}}\right)dt^2$$
$$+ \frac{dR^2}{1 - \frac{2M(t)}{R}} - \frac{2H(t)RdtdR}{1 - \frac{2M(t)}{R}} + R^2 d\Omega^2,\qquad(3)$$

where $H = H(t) = \dot{a}(t)/a(t)$ is the Hubble factor, with $\dot{a}(t)$ standing for the derivative of $a(t)$ with respect to the cosmological time t, and we defined

$$M = M(t) = ma(t).\qquad(4)$$

It is interesting to compare this metric with other proposals in the literature. For instance, in Refs. [21,28] the spacetime metric is given by a generalization of the McVittie solution [1], by letting the mass parameter be a function of the time coordinate. Indeed, the metric of Eq. (2) can be characterized as such a generalized McVittie spacetime with a time-dependent mass parameter $m(t) = ma(t)$. This can be verified by direct comparison between our Eq. (3) and Eq. (9) shown in Ref. [28]. However, the analyses made and the results presented in Refs. [21,28] do not hold integrally for the Thakurta solution we are studying here, because a major part of them relied on the hypothesis that $\dot{m}(t)/m(t) < \dot{a}(t)/a(t)$, while for Thakurta both of such quantities are equal to each other.

Some aspects of metric (2) were analyzed in Ref. [29] (see also Ref. [30]). Note, however, that there has been some confusion concerning the nonrotating Thakurta metric and the Sultana-Dyer metric [31], as pointed out in Ref. [32]. Both are conformal to the Schwarzschild metric,

but they are not the same. The difference between them lies in the dependence of the conformal factor a^2 as a function of the coordinates: in the former it is a function of the *conformal time* η alone, while in the latter it is a function of the *Eddington-Finkelstein advanced time* $u = \eta + 2m \ln|r - 2m|$. This difference is made clear by writing both metrics in diagonal forms as in Eq. (2), when a comparison can easily be performed [see, e.g., Ref. [33] and compare Eq. (2.3) of that paper to our Eq. (2)].

In Ref. [29] the existence of a singularity at $r = 2m$ was discussed, as well as a partial analysis of the causal structure of the related spacetime, considering a scale factor corresponding to a universe filled by dust, given by $a(t) \sim t^{2/3}$, was performed. Also, in [34] a metric of the same type of (2) is considered and some of the results presented in Sec. II of the present work were found. In the present work the analysis of the causal structure for the case $a(t) \sim t^{2/3}$ is completed, and several other forms of the scale factor $a(t)$ are considered. In the following we investigate the main physical and geometrical properties of the corresponding spacetimes. Namely, we investigate the possible matter sources, the global structure, and the causal properties of each spacetime considering different forms of the scale factor $a(t)$.

B. The energy-momentum tensor and the energy conditions

From Eq. (2), it follows that the nonzero components of the energy-momentum tensor $T_\mu{}^\nu$ are given by

$$T_t{}^t = -\frac{3H^2(t)}{8\pi f(R)},$$

$$T_t{}^r = -\frac{f^2(r)}{a^2(t)} T_r{}^t = \frac{M(t)H(t)}{4\pi R^2 a(t)},$$

$$T_r{}^r = T_\theta{}^\theta = T_\varphi{}^\varphi = -\frac{3H^2(t) + 2\dot{H}(t)}{8\pi f(R)}, \qquad (5)$$

where we defined

$$f = f(R) = f(r) = 1 - \frac{2M}{R} = 1 - \frac{2m}{r}. \qquad (6)$$

With relations equation (5) in hand, we can define the kinematic quantities associated to the energy-momentum tensor of the source, which can be modeled as an imperfect isotropic fluid. The flow vector v_μ is given by

$$v_\mu = (-\sqrt{f(R)}, 0, 0, 0),$$

while the orthogonal projector $h_{\mu\nu}$ reads

$$h_{\mu\nu} = \text{diag}(0, a^2(t)f^{-1}(R), R^2, R^2\sin^2\theta).$$

Using the standard definitions for the energy density ρ and pressure p we find

$$\rho \equiv T_{\mu\nu}v^\mu v^\nu = \frac{3H^2(t)}{8\pi f(R)}, \qquad (7)$$

and

$$p \equiv \frac{1}{3}T_{\mu\nu}h^{\mu\nu} = -\frac{3H^2(t) + 2\dot{H}(t)}{8\pi f(R)}. \qquad (8)$$

Also, since the energy-momentum tensor is not diagonal in the tr sub-space, there is a heat flow in the radial direction, whose energy flux is given by

$$q_\sigma = -T_{\mu\nu}v^\mu h^\nu{}_\sigma = \left(0, -\frac{M(t)H(t)}{4\pi a(t)R^2 f^{3/2}(R)}, 0, 0\right). \qquad (9)$$

Therefore, as the source for the rotating Thakurta spacetime [14], a possible source of the nonrotating Thakurta geometry equation (2) is an isotropic fluid with a heat flow in the radial direction. The fluid quantities reduce to those of a homogeneous perfect fluid for large radial coordinate values, as expected. On the other hand, they may diverge at $R = 2M$ which would imply a curvature singularity. This is probably the simplest source for this geometry. However, there are other possible sources, such as a mixture of a perfect fluid and a null fluid, but we do not consider these other more general sources here.

For completeness we state here the energy condition for a fluid with nonzero energy flux. The relevant energy conditions for the present analysis are the null (NEC), weak (WEC) and strong (SEC) energy conditions. Then we have (see, e.g., Ref. [35])

$$\text{NEC} : \rho + p \geq 2|q|, \qquad (10)$$

$$\text{WEC} : \rho - p + \Delta \geq 0, \qquad \rho + p \geq 2|q|, \qquad (11)$$

$$\text{SEC} : \rho + p \geq 2|q|, \qquad 2p + \Delta \geq 0, \qquad (12)$$

where $|q| = |q_\mu q^\mu|$, and

$$\Delta = \sqrt{(\rho + p)^2 - 4|q|^2}. \qquad (13)$$

Using metric (2) and the energy flux vector from Eq. (9) it gives

$$|q| = \frac{M(t)H(t)}{4\pi R^2 f(R)}. \qquad (14)$$

In the analysis of the energy conditions given below, an interesting quantity is the ratio $n(t, r)$ defined by

$$n(t, r) = \frac{\rho + p}{2|q|} = \frac{-\dot{H}(t)R^2}{2MH(t)}. \qquad (15)$$

As seen from the above conditions, a sufficient condition to satisfy, for instance, the NEC is $n(r, t) \geq 1$. Such a quantity shall be used to analyze some of the properties of the trapping horizons in the cases presented below.

C. The Misner-Sharp mass

The Misner-Sharp mass is a measure of the gravitational active mass contained in a given volume of the spacetime (see, e.g., [23]), and may furnish information about the kind of objects enclosed in such a volume. In terms of the areal radius, $R = a(t)r$, the Misner-Sharp mass inside a closed surface of radius R is defined by [24]

$$M_{MS} = \frac{R}{2}(1 - \|\nabla R\|^2). \qquad (16)$$

For the Thakurta metric Eq. (3), it follows

$$\|\nabla R\|^2 = -H^2(t)R^2\left(1 - \frac{2M}{R}\right)^{-1} + 1 - \frac{2M}{R}. \qquad (17)$$

Thus, substituting the last result into Eq. (16) it gives

$$M_{MS} = M + \frac{H^2(t)R^3}{2(1 - \frac{2M}{R})}. \qquad (18)$$

Notice that this expression contains a single concentrate mass contribution, the position-independent term M, which is compatible with the presence of a central object, and another contribution which depends on the radial coordinate, and that can be though of as the energy related to the fluid that fulfills the spacetime, since that second term grows with the Hubble factor. This second contribution resembles the McVittie case [1], with the important difference that in McVittie spacetime the energy density is a homogeneous function.

In order to make this argument more rigorous we can use the decomposition of the Misner-Sharp mass into its Ricci and Weyl parts, E_R and E_W, where the latter is interpreted as the source of the Coulombian part of the gravitational field. Following, e.g., Appendix D of Ref. [36], we obtain the following relation valid for spherically symmetric spacetimes:

$$W^{\alpha\beta\mu\nu}W_{\alpha\beta\mu\nu} = \frac{48E_W^2}{R^6}, \qquad (19)$$

where W is the Weyl tensor. Applying Eq. (19) to the line element (2) we obtain

$$E_W = M = ma(t), \qquad (20)$$

in agreement with our interpretation.

D. The scale factor

In the original Thakurta model [14] the scale factor was not specified, even though it was assumed implicitly that it should describe an expanding cosmological model. Here we keep such an assumption, by imposing that the $a(t)$ function implies a big-bang type expanding model. However, since the mass of the central object increases with $a(t)$, cf. Eq. (20), it is interesting to modify its asymptotic behavior at late times so that the final mass is finite, a necessary condition to have a black-hole type solution. In view of this, we list here the main assumptions on $a(t)$.

(1) Big-bang hypothesis: $\lim_{t\to 0} a(t) = 0$, with monotonically increasing positive $a(t)$.
(2) Expanding hypothesis: $\dot{a}(t)/a(t) \geq 0$.
(3) Cosmologically inspired (unbounded) models:
  (a) Asymptotically de Sitter cosmological model: $a(t) \sim e^{H_0 t}$ for large t.
  (b) Asymptotically CDM model: $a(t) \sim t^{2/3}$.
  (c) Alternative models as stiff matter and cosmic strings fluids, $a(t) \sim t^\alpha$, $\alpha = 1/3$ and $\alpha = 1$.
(4) Bounded models $a(t) \sim$ constant at large t.
  (a) Models with $\dot{a}(t) \gtrsim e^{-t/\tau}$, $\tau > 2m$, at late times— no black holes.
  (b) Models with $\dot{a}(t) \lesssim e^{-t/\tau}$, $\tau < 2m$, large times— black-hole solutions.

III. STRUCTURAL ANALYSIS

A. The curvature singularities

First we analyze all the possible candidates for curvature singularities that might be present in metric (2). Similarly to the Schwarzschild case, the metric is ill defined at $r = 2m$ ($R = 2M$) and $r = 0$ ($R = 0$). Moreover, the points where $a(t)$ vanishes also may be singular points, and a deeper analysis is necessary in order to distinguish between curvature and coordinate singularities.

We start by analyzing the Ricci scalar which is given by

$$\mathcal{R} = R_\mu{}^\mu = \frac{6}{f(R)}(2H^2(t) + \dot{H}(t)). \qquad (21)$$

Since $f(R)$ vanishes at $R = 2M$, it follows that there is a curvature singularity at this point unless the factor between parenthesis, $2H^2(t) + \dot{H}(t)$, vanishes as well. Then, the nature of the metric singularity $R = 2M$ depends on the explicit form of the scale factor $H(t)$. We investigate this point in Sec. IV. Additionally, the Ricci scalar is singular at points where $H(t)$ and/or $\dot{H}(t)$ diverge, what happens, for instance, when the factor $a(t)$ vanishes at a given time, such as in big-bang cosmological models. On the other hand, the Ricci scalar is nonsingular at $R = 0$, and hence the behavior of the other curvature scalars at that point has to be analyzed.

The Kretschmann scalar $\mathcal{K}$ is

$$\mathcal{K} = R^{\alpha\beta\gamma\delta} R_{\alpha\beta\gamma\delta} = \frac{12}{f^2(R)} (H^4 + (H^2 + \dot{H})^2)$$
$$+ \frac{16M^2}{R^4} \left(\frac{3}{R^2} - \frac{H^2}{f^2(R)} \right), \tag{22}$$

showing that $R = 0$ is a curvature singularity. Recalling that $R = ra(t)$, this includes the locus where $r = 0$ and the points where $a(t) = 0$, i.e., at the initial time in a big-bang cosmological scenario [where also $H(t), \dot{H}(t) \to \infty$]. Moreover, it results that $R = 2M$ is a curvature singularity whenever $H(t) \neq 0$ and $\dot{H}(t) \neq 0$.

B. Trapping horizons

Following Ref. [22], we classify any sphere of symmetry S of the spacetime according to the expansions $\Theta_\pm$ of the null congruences defined by outgoing and ingoing null rays, as follows:

(1) if $\Theta_+\Theta_- < 0$, we say that S is *regular*;
(2) if $\Theta_+\Theta_- > 0$, with $\Theta_\pm < 0$, we say that S is *trapped*;
(3) if $\Theta_+\Theta_- > 0$, with $\Theta_\pm > 0$, we say that S is *antitrapped*;
(4) if $\Theta_+\Theta_- = 0$, then we say that S is *marginal*.

This classification divides the spacetime in regions composed by each type of sphere. When drawing figures representing spacetime diagrams we indicate the different regions using the signs of expansions between parenthesis. Namely, we use $(--)$ to indicate trapped regions, $(+-)$ to indicate regular regions, and $(++)$ to indicate antitrapped regions.

A *trapping horizon* is defined as the tube foliated by marginal spheres. In the case of a spherically symmetric metric such as Eq. (3), these are given by the solutions of the equations

$$\Theta_\pm = \frac{2}{R} k_\pm^a \nabla_a R = 0, \tag{23}$$

and we get

$$H(t)R_\pm(t) \pm \left(1 - \frac{2M(t)}{R_\pm(t)} \right) = 0, \tag{24}$$

where the $\pm$ sign refers to outgoing (ingoing) null geodesics.

Taking $H(t) > 0$ it follows from Eq. (24) that in the $R > 2M(t)$ region there are real solutions only for the ingoing expansion (minus sign) equation. Conversely, for $R < 2M(t)$ the real solutions only exist for the outgoing expansion (plus sign) equation. Thus, only ingoing geodesics have vanishing expansion in the $R > 2M(t)$ region, which is the region of interest for the present analysis. The equation for the expansion of the ingoing null geodesics

then yields two solutions for the trapping horizons, that we denote with an overhead hat throughout this paper,

$$\hat{R}_\pm(t) = \frac{1}{2H(t)} (1 \pm \sqrt{1 - 8M(t)H(t)}). \tag{25}$$

The subsequent study of geodesic completeness and of causal structure is simplified by using the original coordinates, i.e., in terms of the comoving radial coordinate r, and then it is useful to write the relations defining the trapping horizons in terms of r. Using the relations $R = ra(t)$ and $M(t) = ma(t)$, Eq. (25) can be cast into the form

$$\hat{r}_\pm = \frac{1}{2\dot{a}} (1 \pm \sqrt{1 - 8m\dot{a}}) = \frac{4m}{1 \mp \sqrt{1 - 8m\dot{a}}}. \tag{26}$$

It is seen that $\hat{r}_\pm$ are always larger than $2m$, $\hat{r}_\pm > 2m$ for $\dot{a} \neq 0$. In the case $\dot{a}$ vanishes the horizon $\hat{r}_-$ satisfies the equality $\hat{r}_- = 2m$ while $\hat{r}_+$ reaches arbitrarily large values. Here we refer to the loci defined by the images of the curves $\hat{r}_\pm(t)$ as the outer $(+)$ and the inner $(-)$ horizons, respectively, since $\hat{r}_-(t) \leq \hat{r}_+(t)$, $\forall\, t > 0$ for which the trapping horizons exist.

Notice that both horizons only exist as long as $\dot{a} < \frac{1}{8m}$, which provides very different structures depending on the behavior of the scale factor $a(t)$. Therefore, the trapping horizons can be roughly traced to the behavior of a, that we divide into three broad classes[1]:

(a) For large t, $\dot{a} > 1/8m$, then the trapping horizons have a finite life span, forming a closed curve and defining a bounded region in the (t, r) plane in its interior. For instance, considering the scale factor $a = \sinh^{2/3}(3H_0 t/2)$, as an asymptotic ΛCDM model, as showed in Fig. 1.

(b) For large t, $\dot{a} < 1/8m$, then the trapping horizons are formed some time after the big bang and remain for arbitrarily large t, dividing first quadrant of the (t, r) plan in two open, unbounded regions. For instance, considering the scalar factor $a = (t/t_0)^{2/3}$, as in the dust cosmological model, as showed in Fig. 2.

(c) For large t, $\dot{a} \leq 1/8m$ and, moreover, $\dot{a} \leq 1/8m$ at initial times, then the trapping horizons are formed at the big bang and remain for arbitrarily large t, dividing the first quadrant of the (t, r) plan into three open, unbounded regions. For instance, considering the scalar factor $a = \tanh(t/t_0)$, with $t_0 \geq 8m$ as showed in Fig. 3. In the case $\dot{a} = 1/8m$ for all times the two trapping horizons coincide. This is a particular case of linear scale factors $a(t) \sim t$ which are analyzed in the next section.

---

[1]Here, we choose to not consider cases where $\dot{a}(t)$ oscillates between values below and above $1/8m$. In those cases the trapping horizons could form an arbitrary number of regular bubbles dividing the spacetime in an arbitrary number of regions.
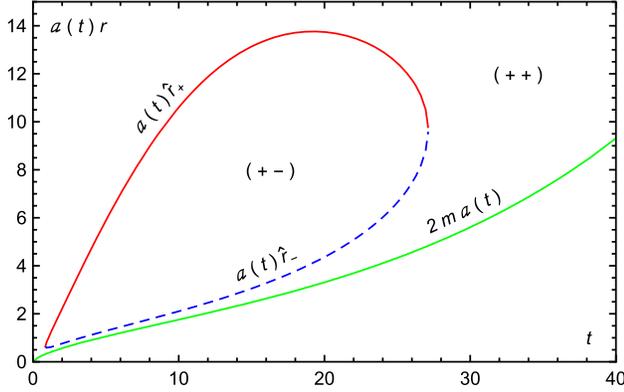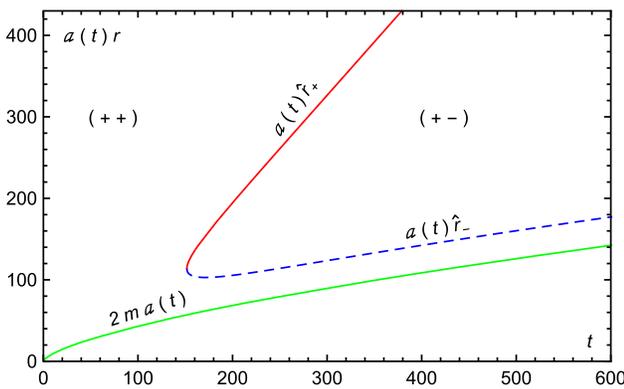
FIG. 1. The outer ($\hat{R}_+ = a(t)\hat{r}_+$) and inner ($\hat{R}_- = a(t)\hat{r}_-$) horizons represented by red (solid) and blue (dashed) lines, respectively, as given by Eq. (25). Here the scale factor is $a(t) = \sinh^{2/3}(3H_0 t/2)$, with $H_0 = 0.05$, and the mass parameter was set to unity, $m = 1$. The curve $R = 2ma(t)$ is also represented by the lowermost green (solid) line.

C. Geodesic completeness

In order to characterize the spacetime described by the Thakurta metric, we need to investigate the characteristics of the patch covered by the given coordinates. A very important property that we must verify is if the limits of the region covered by the chosen coordinates are at finite or infinite proper distance of the events at finite coordinates. In other words, we must check the geodesic completeness. For that we study the asymptotic behavior of the affine parameter as the time coordinate t tends to infinity (future behavior), and to zero (past behavior) along the null geodesics.

1. Future behavior of null geodesics

The outgoing null geodesics are trivially future complete ($t \to \infty$), since the spacetime is asymptotically FLRW as
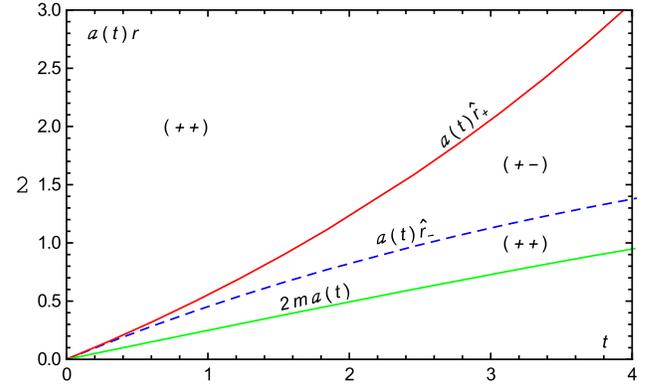

FIG. 2. The outer ($\hat{R}_+ = a(t)\hat{r}_+$) and inner ($\hat{R}_- = a(t)\hat{r}_-$) horizons represented by red (solid) and blue (dashed) lines, respectively, as given by Eq. (25). Here the scale factor is $a(t) = (t/t_0)^{2/3}$, with $t_0 = 1$, and the mass parameter was set to unity, $m = 1$. The curve $R = 2ma(t)$ is also represented by the lowermost green (solid) line.

FIG. 3. The outer ($\hat{R}_+ = a(t)\hat{r}_+$) and inner ($\hat{R}_- = a(t)\hat{r}_-$) horizons represented by red (solid) and blue (dashed) lines, respectively, as given by Eq. (25). Here the scale factor is $a(t) = \tanh(t/t_0)$, with $t_0 = 8m$, and the mass parameter was set to $m = 1.25$. The curve $R = 2ma(t)$ is also represented by the lowermost green (solid) line.

$r \to \infty$ and its results can be used. Therefore, we have to verify completeness for ingoing null geodesics, which approach $r = 2m$. For that we consider the equation for ingoing null geodesics in terms of the affine parameter λ,

$$r'_- = -\frac{t'}{a}\left(1 - \frac{2m}{r_-}\right), \tag{27}$$

$$t'' = \left(\frac{2m}{ar_-^2} - H\right)t'^2, \tag{28}$$

where the prime stands for the λ-derivative.

Equation (27) can be rewritten in terms of the conformal time $d\eta = dt/a$ and integrated to produce

$$r_- + 2m\ln(r_- - 2m) = -\eta + C, \tag{29}$$

where C is an arbitrary constant.

In order to analyze geodesic completeness, we study the behavior of the affine parameter as t tends to infinity along ingoing null geodesics. Using Eq. (28) we obtain for large t,

$$\frac{t''}{t'} \approx K\frac{t'}{a} - \frac{\dot{a}t'}{a}, \tag{30}$$

where we defined $K \equiv \frac{2m}{r_\infty^2}$, with r_∞ denoting the value of $r_-(t)$ in the limit of large times. Integrating Eq. (30) we have

$$\ln t' \approx K\eta(t) - \ln a + \text{constant}. \tag{31}$$

Then the parameter λ is given by the integration of Eq. (31) as
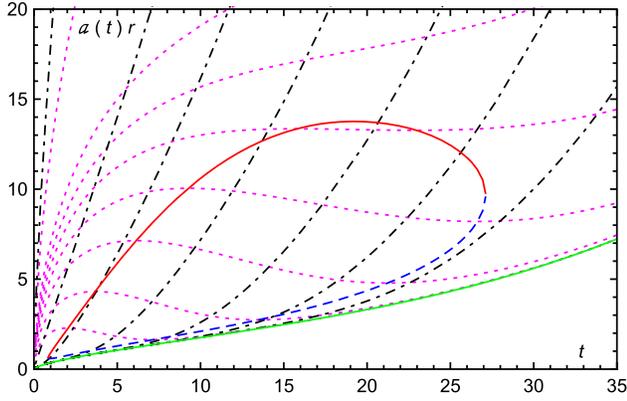
FIG. 4. Ingoing and outgoing geodesics represented by magenta (dotted) and black (dotted-dashed) lines, respectively. The scale factor is $a(t) = \sinh^{2/3}(3H_0 t/2)$, with $H_0 = 0.05$. The outer/inner horizons and the $r = 2m$ curve are represented respectively by the blue (solid), red (dashed) and green (solid, lowermost) lines. The mass parameter m has been set to unity.
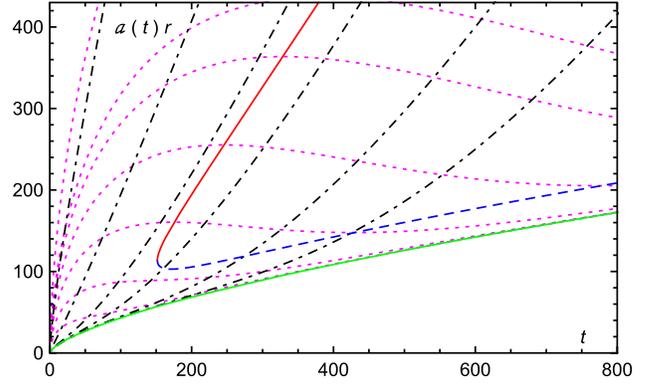

FIG. 5. Ingoing and outgoing geodesics represented by magenta (dotted) and black (dotted-dashed) lines, respectively, for the case $a(t) = (t/t_0)^{2/3}$, with $t_0 = 1$. The outer/inner horizons and the $R = 2ma(t)$ curve are represented respectively by the blue (solid), red (dashed) and green (solid, lowermost) lines. The mass parameter m has been put to unity.

$$\lambda(t) \sim \int^t e^{-K\eta(u)} a(u) \mathrm{d}u, \qquad (32)$$

and the convergence or divergence of the last integral as $t \to \infty$ determines if the spacetime is geodesically incomplete or complete, respectively. A more cautious proof of this result, considering the effect of subleading terms, is the subject of Appendix C.

The convergence of the integral in Eq. (32) depends on η, and we must consider the two aforementioned possibilities.

  (i) $\eta(t)$ is bounded as $t \to \infty$.
  (ii) $\eta(t)$ is unbounded as $t \to \infty$.

If η is bounded, case i, Eq. (29) implies that the surface $r = 2m$ is unreachable by ingoing null geodesics. This behavior can be seen in Fig. 4 as, for example, taking $a(t) = \sinh^{2/3}(3H_0 t/2)$. Thus, defining $\eta_\infty = \lim_{t\to\infty}\eta(t)$ we can define $r_\infty \equiv r_-(\eta_\infty) > 2m$. In terms of the areal radius we have $R_-(t) \sim a(t)r_\infty$ for large t, which implies that the expansion of ingoing geodesics is positive in this limit.

Thus, we have that $\eta(t) < \eta_\infty$, for all $t > 0$, such that

$$\lambda \sim \int^\infty e^{-K\eta(u)} a(u) \mathrm{d}u > e^{-K\eta_\infty} \int^\infty a(u) \mathrm{d}u \to \infty, \quad (33)$$

hence, if $\eta(t)$ is bounded, the Thakurta spacetime is future geodesically complete.

On the other hand, in case ii, the limit of the null ingoing geodesics as $t \to \infty$ is $r_\infty = 2m$. In order to address this case we analyze the particular situation where the scale factor is asymptotically linear, $a(t) \sim a_0 t$ for large t. In this case we have, for large t,

$$\lambda \sim \int^\infty e^{-\frac{K \ln(u)}{a_0}} u \mathrm{d}u = \int \frac{1}{u^{\frac{K}{a_0}-1}} \mathrm{d}u. \qquad (34)$$

Therefore, the convergence depends on the difference $\frac{K}{a_0} - 1 = \frac{1}{2a_0 m} - 1$. Moreover, since $K \equiv 2m/r_\infty^2$ we obtain

$$\frac{1}{2a_0 m} - 1 \leq 1 \Leftrightarrow a_0 m \geq 1/4 \Rightarrow \lambda \to \infty \quad \text{(complete)}, \tag{35}$$

$$\frac{1}{2a_0 m} - 1 > 1 \Leftrightarrow a_0 m < 1/4 \Rightarrow \lambda < \infty \quad \text{(incomplete)}. \tag{36}$$

By extension, we conclude that in case ii, the Thakurta spacetime is geodesically complete if, for large t, $a(t) > \frac{t}{4m}$ and geodesically incomplete if $a(t) < \frac{t}{4m}$. In particular, this implies that all Thakurta spacetimes with sublinear $a(t)$ are geodesically incomplete, as for example $a(t) = (t/t_0)^{2/3}$ showed in Fig. 5.

2. Past behavior of null geodesics

Here we show that the singularity $a(t) = 0$ is always at a finite time in the past for all models we consider in this work. For this we study the behavior of the null geodesics in the limit $t \to 0$.

For ingoing null geodesics we must consider Eqs. (28) and (29). Following a similar reasoning used in the study of the future behavior of null geodesics, we find that if η is bounded from below then $r_-(t)$ is bounded, i.e., $2m < r_-(t) < r_{\max}$, while if η is unbounded $r_-(t) \to \infty$ as $a(t) \to 0$, which means that, by Eq. (29), we can use the approximation $r_-(\eta) \sim -\eta$.

First, we consider the bounded case, for which $r \to r_{\max}$ as $t \to 0$. We can choose $\eta(t = 0) = 0$ with no loss of generality. The procedure is analogous to the one used to investigate completeness to the future, since the behavior is

governed by Eq. (28). Redefining $K = \frac{2m}{r_{max}^2} > 0$ in Eq. (30) and integrating, we obtain

$$\Delta\lambda \approx \int_t^0 \exp\left[-K\eta(u)\right]a(u)\mathrm{d}u. \qquad (37)$$

Since $\eta(t) \geq 0$ and $K > 0$, it follows $\exp\left[-K\eta(u)\right] \leq 1$, and hence

$$|\Delta\lambda| \leq |\int_t^0 a(u)\mathrm{d}u|, \qquad (38)$$

which is always finite.

Similarly, if η is unbounded from below, $\lim_{t\to 0}\eta(t) = -\infty$, we obtain, instead of Eq. (37), the following relation:

$$\Delta\lambda \approx \int_t^0 \exp\left(\frac{2m}{\eta(u)}\right)a(u)\mathrm{d}u, \qquad (39)$$

which is always finite, since $\exp(\frac{2m}{\eta(u)}) \leq 1$ for $\eta(u) < 0$.

Therefore, all the ingoing null geodesics are incomplete to the past, which proves that the surface $a(t) = 0$ is a singularity in the past of all events in Thakurta spacetimes, and it is justified to call it a big-bang singularity in this context.

Using similar arguments we can also prove that the outgoing null geodesics are incomplete to the past.

D. Conformal boundaries

In order to build the conformal diagrams of the Thakurta spacetimes, we have to study the properties of the conformal boundaries at the past $a(t) \to 0$ and at the future $t \to \infty$. Using the conformal time coordinate $\eta = \int \frac{\mathrm{d}t}{a(t)}$ and the tortoise coordinate $r^* = \int \frac{\mathrm{d}r}{f(r)}$, the Thakurta metric can be written in the form

$$\mathrm{d}s^2 = a^2(\eta)f(r)(-\mathrm{d}\eta^2 + \mathrm{d}r^{*2} + r^2(r^*)\mathrm{d}\Omega), \qquad (40)$$

which is conformally flat in the (η, r^*) submanifold. Since $-\infty < r^* < \infty$, the behavior of η as $t \to 0$ determines the properties of the $a(t) = 0$ surface in the past, as in the FLRW models [37,38].

(1) If $\lim_{a(t)\to 0}\eta(t)$ is finite, then the Thakurta spacetime is conformally related to a portion of Minkowski spacetime at the future of a constant time spacelike hypersurface. This implies that the past conformal boundary is spacelike.

(2) If $\lim_{a(t)\to 0}\eta(t) = -\infty$, then the past conformal boundary of the Thakurta spacetime corresponds to the boundary of the Minkowski spacetime and it is null.

Analogously, we have the same two cases in the limit $t \to \infty$ for the future boundary:

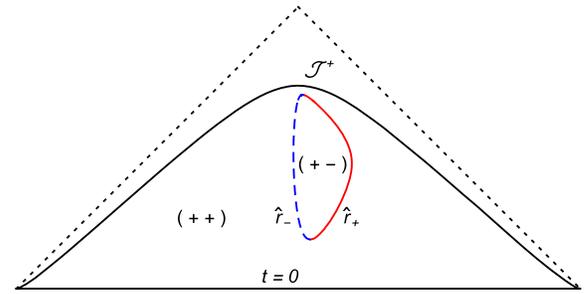FIG. 6. The causal diagram for a ΛCDM model where $a(t) = \sinh^{2/3}(3H_0 t/2)$, with $mH_0 = 0.03$. There is a spacelike initial singularity at $t = 0$. Also the conformal time η is bounded and the future infinity is spacelike. The dotted lines are not part of the spacetime and are drawn for comparison to the other situations.

(1) If $\lim_{t\to\infty}\eta(t)$ is finite, then the Thakurta spacetime is conformally related to a portion of the Minkowski spacetime at the past of a constant time spacelike surface. The future boundary is spacelike in this case, as in the particular sample depicted in Fig. 6.

(2) If $\lim_{t\to\infty}\eta(t) = \infty$, then the future conformal boundary of the Thakurta spacetime corresponds to the boundary of the Minkowski spacetime and it is null.

Therefore, by choosing the asymptotic behavior of the function $a(t)$ in the future and in the past we can build Thakurta models with the four possible combinations in terms of conformal boundaries. We shall show below some examples of topologies given by different examples of $a(t)$.

IV. THE SURFACE AT $R = 2M$

In Sec. III C, we stated the conditions on $a(t)$ that imply the surface $r = 2m$ is reached in a finite affine parameter by null ingoing geodesics.

We need to evaluate the properties of that surface, namely, if it is singular or regular. Since the Ricci scalar is given by Eq. (21), it may diverge as $t \to \infty$ and $r \to 2m$. In order to determine whether that divergence of the Ricci scalar is physical or not, we evaluate its limit along some classes of physical trajectories.

A. Null trajectories

The null ingoing geodesics satisfy the relation given in Eq. (29). Near the $r \to 2m$ limit it can be approximated by

$$r_- \approx 2m + C'\exp\left(\frac{-\eta}{2m}\right), \qquad (41)$$

which leads to

$$f[r_-(\eta)] \sim \frac{C'}{2m}\exp\left(\frac{-\eta}{2m}\right). \qquad (42)$$

Therefore, the Ricci scalar is given by

$$\mathcal{R} \sim \exp\left(\frac{\eta}{2m}\right) \times \frac{\dot{a}^2 + a\ddot{a}}{a^2}. \tag{43}$$

If we assume that $a(t)$ behaves asymptotically as a power of t, $a(t) \sim t^\alpha$ with $\alpha > 0$, it follows $a(\eta) \sim \eta^{\frac{\alpha}{1-\alpha}}$ and thus, if $\dot{a}^2 + a\ddot{a} \neq 0$, $\mathcal{R} \to \infty$ since the exponential dominates as $\eta \to \infty$. The form of the scale function that provides $\dot{a}^2 + a\ddot{a} = 0$ is $a(t) = c_1 t^{1/2}$. In this case, the singularity appears in the Kretschmann scalar (22), which in the limit $r \to 2m$ goes as $\mathcal{K} \sim \exp(\frac{\eta}{m}) \times \eta^{-8}$ and that also diverges in the limit $\eta \to \infty$.

The conclusion is that the surface $r = 2m$ is singular for lightlike geodesics if the scale factor grows as a power law (or at a higher rate) at large cosmological times.

B. Timelike observers

Lightlike (null) trajectories are the fastest allowed paths for sign travel in general relativity, and hence it would be interesting to check if the analysis performed in Sec. IV A would give a different result if we used timelike trajectories, that move at lower velocities.

Here it is convenient to use the conformal time η as the time coordinate, bringing the line element to the form given in Eq. (2).

We can parametrize the 4-velocity of any timelike observer as

$$u^0 = \frac{d\eta}{ds} = \frac{\cosh\omega}{a\sqrt{f(r)}}, \quad u^1 = \frac{dr}{ds} = \frac{\sqrt{f(r)}\sinh\omega}{a}, \tag{44}$$

where s is the proper time of the observer and ω is its *rapidity*. Therefore, we have

$$\frac{dr}{d\eta} = \frac{u^1}{u^0} = f(r)\tanh\omega, \tag{45}$$

which gives

$$\eta(r) = \int \frac{dr}{f(r)\tanh\omega}. \tag{46}$$

Since we are interested in ingoing observers that reach the $r = 2m$ surface at a finite proper time, it is appropriate to take $\omega = -|\omega|$. In order to simplify the problem further, we consider that ω is constant along the trajectory. Then we obtain

$$\eta = -\frac{1}{\tanh|\omega|}(r + 2m\ln(r - 2m)) + \text{constant}, \tag{47}$$

and hence, close to the limit $r \to 2m$, it yields

$$r(\eta) \sim C\exp\left(-\frac{\eta\tanh|\omega|}{2m}\right) + 2m. \tag{48}$$

Next we find the approximate form for the function $f(r)$ along a timelike geodesic in the limit $r \to 2m$,

$$f[r(\eta)] \sim \exp\left(-\frac{\eta\tanh|\omega|}{2m}\right). \tag{49}$$

From these results, and with the hypothesis that $a(t)$ behaves asymptotically as a power of t, it is seen that f dominates the limit of $\mathcal{R}$ as $\eta \to \infty$, irrespective of the value of $|\omega|$, and the timelike geodesics hit a singularity ($\mathcal{R} \to \infty$) at $r = 2m$.

This proof also applies for ingoing observers with variable ω provided $|\omega|$ is bounded from below.

C. Building Thakurta models with a nonsingular $r = 2m$ surface

As seen from the previous analysis, the Thakurta metric does not correspond to a black-hole spacetime if the scale factor follows the standard cosmological scenario. Notice that in order to obtain a black-hole model from that metric, it has to be associated to an incomplete patch of the spacetime and the locus $r = 2m$ must be a nonsingular surface, which would be the expected locus of the event horizon.

The above analysis suggests that, as $f[r(t)]$ goes to zero exponentially for timelike and null lines, the derivatives of $a(t)$ should also vanish exponentially fast in a time scale shorter than that of $f[r(t)]$. This also implies that $a(t)$ has to be bound as $t \to \infty$, and hence all models where $a(t)$ is unbounded are singular at $r = 2m$. Then we assume here that $\lim_{t\to\infty} a(t) = a_\infty > 0$. In this case, the conformal time behaves linearly with respect to the cosmic time, that is, $\eta \sim t/a_\infty$ for large times.

Consider now the Kretschmann scalar, which is given by Eq. (22). The dominant term in $\mathcal{K}$ in the limit $r \to 2m$ is $\dot{a}^2/f^2[r(t)]$. Thus, in order to have a finite $\mathcal{K}$, assuming $\dot{a} \sim e^{-t/\tau}$, the constraint

$$\frac{1}{2m} - \frac{2}{\tau} < 0 \Leftrightarrow \tau < 4m, \tag{50}$$

must be satisfied. Therefore, a sufficient condition for the surface $r = 2m$ being nonsingular is $\dot{a} < \mathcal{O}(e^{-t/4m})$. This condition may be fulfilled by models with $a(t) = \tanh(t/t_0)$ studied in Sec. V, if $t_0 = 2\tau < 8m$. In cases like this the spacetime can be extended across the surface $r = 2m$ and its analytical extension may be a black-hole or white-hole spacetime.

V. ANALYSIS OF SOURCES AND CAUSAL STRUCTURE

A. Preliminaries

Different models can be crafted for different choices of $a(t)$. The main differences between them are related to the

existence or not of a singularity at $r = 2m$, and the behavior of the geodesics going to both time boundaries (past singularity and future time infinity). We shall then present some examples of interesting cases with different causal structures. In all the examples discussed in this section the value of the mass parameter is fixed to $m = 1$.

B. Solutions with unbounded scale factor

1. Preliminaries

Let us start with a few examples of scale factors that may describe some phase of expanding cosmological models. In all of the cases studied in this section the function $a(t)$ starts with zero value at $t = 0$, a big-bang type singularity, and growths monotonically with the cosmological time.

2. $a(t) = \sinh^{3/2}(t/t_0)$: A smooth ΛCDM model

The first case is a ΛCDM universe with $a(t) = \sinh^{2/3}(t/t_0)$, $t_0 = 2/(3H_0)$, as the model used in Ref. [19]. In this case the central mass $M(t) = ma(t)$ grows exponentially fast at late times. The horizons exist only by a finite amount of time and form a bubble that does not reach the future infinity, as represented in Fig. 1.

The causal diagram depicted in Fig. 6 summarizes the geometrical properties of the corresponding spacetime. The locus $r = 2m$ is beyond the future infinity and the space-time presents a bounded conformal time η, which is represented by the spacelike (black, solid) curve delimiting the spacetime. The regular region lies inside the closed surface generated by the trapping horizons, the surface $t = 0$ is spacelike (and singular), and the spacetime is future geodesically complete. No black hole is present, and the shown diagram is in fact the maximal analytical extension.

The choice $a(t) = \sinh^{2/3}(3H_0t/2)$ is motivated by the standard cosmological scenario, which has a phase dominated by cold dark matter (dust fluid, $p = 0$) and approaches a de Sitter fluid ($p = -\rho$) at late times, and has been used in Refs. [19,20]. The related energy density and pressure [see Eqs. (7) and (8)] are given respectively by

$$8\pi\rho = \frac{3H_0^2\coth^2[3H_0t/3]}{f(r)}, \qquad 8\pi p = -\frac{3H_0^2}{f(r)}, \quad (51)$$

where $f(r)$ is given by Eq. (6).

Since the pressure is time independent, the ratio $w(t) = p/\rho$, plotted in Fig. 7, indicates the time evolution of the energy density. At early times the energy density is large, the fluid behaves like a dust fluid, while at late times the energy density is also a constant. The final state is $p = -\rho = -3H_0^2/(1 - \frac{2m}{r})$.

The only nonzero component of the heat flow q_μ is the one along the radial direction, q_r. Eq. (14) then gives
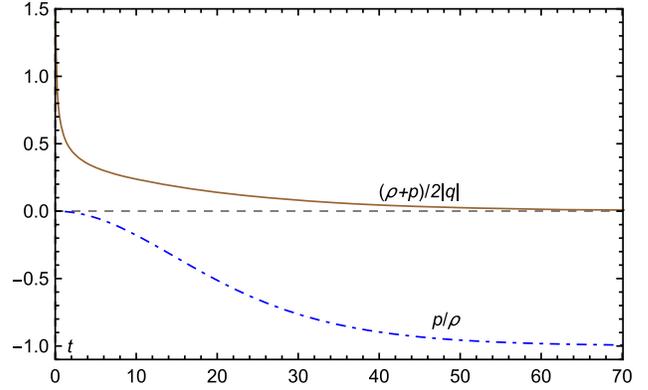

FIG. 7. The curves for $w(t) = p/\rho$ and $(p + \rho)/2|q|$ in the case $a(t) = \sinh^{2/3}(3H_0t/2)$, for $H_0 = 0.03$ and $r = 3 \times m$ (we have chosen $m = 1$).

$$|q| = \frac{2mH_0 \coth(3H_0t/2)}{r^2\sinh^{5/3}(3H_0t/2)f(r)}, \qquad (52)$$

where $f(r)$ is given by Eq. (6). This energy flux decreases with r^{-2}, it is arbitrarily large at initial times and tends to zero at late times.

The energy density and pressure, given by Eq. (51), together with the energy flux (52), define the energy-momentum content of the spacetime. Regarding to the energy conditions [cf. Eqs. (10), (11), and (12)] the important quantity to analyze is ratio $n(t, r) = (\rho + p)/2|q|$, defined in Eq. (15), which in the present case is $n(t, r) = \frac{3H_0r^2}{2m}\text{csch}(3H_0t)\sinh^{2/3}(3H_0t/2)$, and so the energy conditions strongly depend on time and radial coordinates. For small times it approaches to $n(t, r) \sim 9r^2H_0^{2/3}/(4mt^{1/3})$, while for large times it results $n(t, r) \sim 3r^2H_0e^{-H_0t}/(2m)$. Hence, at very initial times and finite $r > 2m$, the constraint $\rho + p \geq 2|q|$ holds and it can be verified that all the energy conditions are satisfied. Moreover, since (for fixed r) the function $\rho + p$ vanishes faster than the energy flux $|q|$, at late times (for fixed r) the constraint $\rho + p \geq 2|q|$ does not hold and the NEC, the WEC, and the SEC are violated. Such a behavior is depicted in Fig. 7. On the other hand, since $|q|$ falls with $1/r^2$, for any fixed time, at sufficiently large radial coordinates ($r \to \infty$), the NEC, the WEC, and the SEC are satisfied.

We can also evaluate the energy conditions along the trapping horizons $\hat{r}_+(t)$ and $\hat{r}_-(t)$, and investigate the character of the trapping horizons in the spirit of the classification and theorems of Refs. [22] and [39]. To do that properly, and to be able to compare the different cases, we report on such a subject in Appendix D.

3. $a(t) = (t/t_0)^{2/3}$: CDM (dust fluid) model

Another important example is a dust model with $a(t) = (t/t_0)^{2/3}$ for all $t > 0$. For this scale factor the trapping
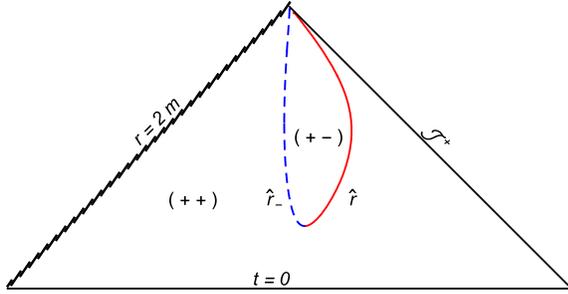
FIG. 8. The causal diagram for the dust model $a(t) = (t/t_0)^{2/3}$, with $t_0 = 1 = m$. There is an initial singularity at $t = 0$, a null singularity at $r = 2m$. The trapping horizons are timelike for large times.

FIG. 9. The curve for $\rho/2|q|$ in the case $a(t) = (t/t_0)^{2/3}$, with $t_0 = 1$ and $r = 2.5 \times m$ (we have chosen $m = 1$).

horizons have similar forms to those presented in Fig. 2. Here the conformal time η is unbounded and hence the lightlike geodesics reach the future null infinity. At late times both of the horizons are timelike and form a closed curve that reaches the timelike infinity. The causal diagram is given in Fig. 8.

Similarly to the case of the last section, the regular region is inside the closed curved formed by the trapping horizons. The surface $t = 0$ is singular and spacelike. An important difference is that here the lightlike surface $r = 2m$ belongs to the spacetime, it is a singular boundary of the spacetime. Moreover, the spacetime is geodesically incomplete also to the future, for geodesics hitting the singularity at $r = 2m$. The Fig. 8 then shows the maximal analytical extension of the solution.

The $a(t) = (t/t_0)^{2/3}$ function produces a dust background fluid with a heat flow in the radial direction,

$$8\pi\rho = \frac{4}{3t^2}\frac{1}{f(r)}, \qquad 8\pi p = 0,$$

$$8\pi|q| = \frac{4mt_0^{2/3}}{3t^{5/3}}\frac{1}{r^2 f(r)}, \qquad (53)$$

where $f(r)$ is given by Eq. (6). Since the properties of this fluid are very simple we do not show the graphs of the fluid quantities nor of the ratio p/ρ for this case.

The energy density, the pressure, and the energy flux are given by Eq. (53). As in the case of the last section, the energy conditions are satisfied at early times, but the heat flux decreases slower than the energy density and dominates for large times. Such a behavior is depicted in Fig. 9. In the present case Eq. (15) yields $n(t, r) = (\rho + p)/2|q| = r^2/(mt_0^{2/3}t^{1/3})$. At very initial times (and fixed $r > 2m$), the constraint $\rho + p \geq 2|q|$ holds and it can be verified that all the energy conditions are satisfied. Moreover, since the function $\rho + p$ vanishes faster than the energy flux $|q|$ with t, at late times (and fixed $r > 2m$) the constraint $\rho + p \geq 2|q|$ does not hold and the NEC, the WEC, and the SEC are violated. On the other hand, since
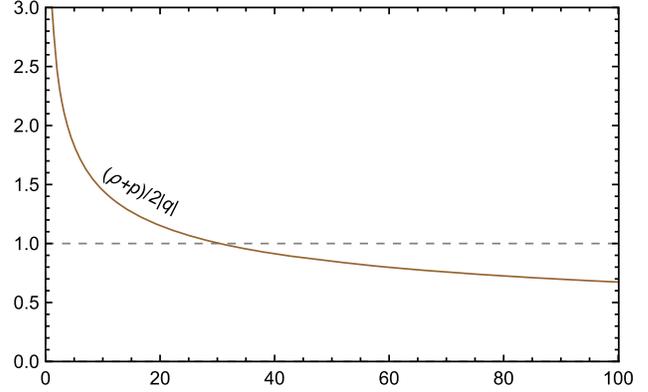
$|q|$ falls with $1/r^2$, for any fixed time at sufficiently large radial coordinates ($r \to \infty$), the NEC, the WEC, and the SEC are satisfied.

Some details of the energy conditions along the trapping horizons and their properties are given in Appendix D.

4. $a(t) = (t/t_0)^{1/3}$: Stiff matter model

In some cosmological models there is a "stiff matter" era [40], notably when dark matter is modeled as Bose-Einstein condensates, where the equation of state is $\rho = p$. A stiff matter model with positive energy is considered with $a(t) = (t/t_0)^{1/3}$, yielding an unbounded conformal time η. At late times the inner trapping horizon is timelike while the outer trapping horizons is spacelike for all times. The inner horizon changes to the spacelike character at a given intermediate time. The causal structure is presented in Fig. 10. As in the last two cases, the initial singularity $t = 0$ is spacelike. Here, as in the case of dust matter, the surface $r = 2m$ is singular and the spacetime is also future geodesically incomplete.

The energy density, the pressure, and the energy flux for stiff matter model are given respectively by
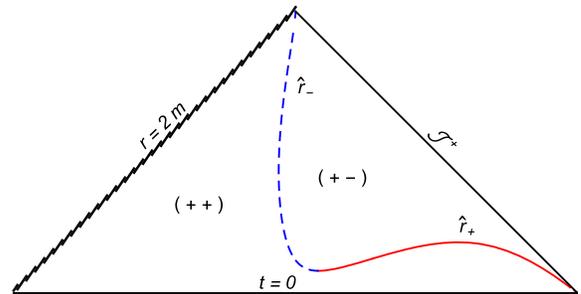

FIG. 10. The causal diagram for the stiff matter model with $a(t) = (t/t_0)^{1/3}$, with $t_0 = 1 = m$. The spacetime is geodesically incomplete with $r = 2m$ and $t = 0$ being singular surfaces. At late times, the inner trapping horizon is timelike while the outer horizon is spacelike.
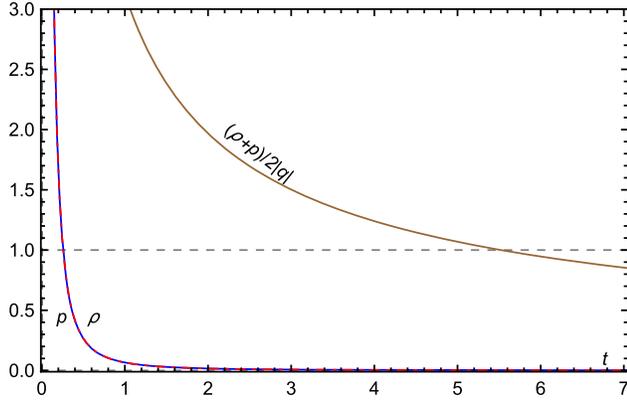
FIG. 11. The energy density, the pressure, and the ratio $(\rho + p)/2|q|$ from Eq. (54), with $r = 2.5m$ and $m = 1$, for the case $a(t) = (t/t_0)^{1/3}$, with $t_0 = 1$.

$$8\pi\rho = 8\pi p = \frac{1}{t^2 f(r)}, \qquad |q| = \frac{2m}{3t_0^{1/3} t^{4/3}} \frac{1}{r^2 f(r)}, \qquad (54)$$

where $f(r)$ is given by Eq. (6). The curves for ρ and p as a function of the cosmological time (for fixed r) are shown in Fig. 11 (they are identical). The ratio $n(t,r) = (\rho + p)/2|q| = r^2/ \times (2mt_0^{1/3}t^{2/3})$ is also shown in that figure.

As seen from the curves for $(\rho + p)/2|q|$ in Figs. 9 and 11, the situation here is very similar to the case of dust matter reported in the last subsection. We note that for early times the ratio $n(t,r)$ is grater than unity, and we can show that the energy conditions are satisfied, while for late times the ratio becomes smaller than unity, so that the condition $(\rho + p) - 2|q| \geq 0$ does not hold and the energy conditions are violated. The curves shown in Fig. 11 depend also upon the radial coordinate r, so that for very large r and finite t the energy conditions are satisfied. For the behavior of the energy conditions on the trapping horizons see Appendix D.

5. $a(t) = (t/t_0)$: Fluid of cosmic strings model

A particularly intriguing case is when $a(t) = (t/t_0)$, where the mass function $M(t) = ma(t)$ increases linearly with the time t.

Taking $t_0 > 8m$ the trapping horizons are created with the big bang at $t = 0$ and persist for all times up to $t \to \infty$, being timelike for all times. The initial singularity is lightlike, and the locus $r = 2m$ is singular, as indicated in the causal diagram depicted in Fig. 12. The spacetime is geodesically incomplete to the future, but all the incomplete geodesics terminate at the singularity $r = 2m$.

The special case with $t_0 = 8m$ presents just one trapping horizon [the two solutions $\hat{r}_\pm(t)$ coincide], the regular region $(+-)$ disappears but the conformal boundaries are the same as for $t_0 > 8m$, as depicted in Fig. 12. On the other hand, for $t_0 < 8m$ there are no trapping horizons and this situation is not considered in the present analysis.
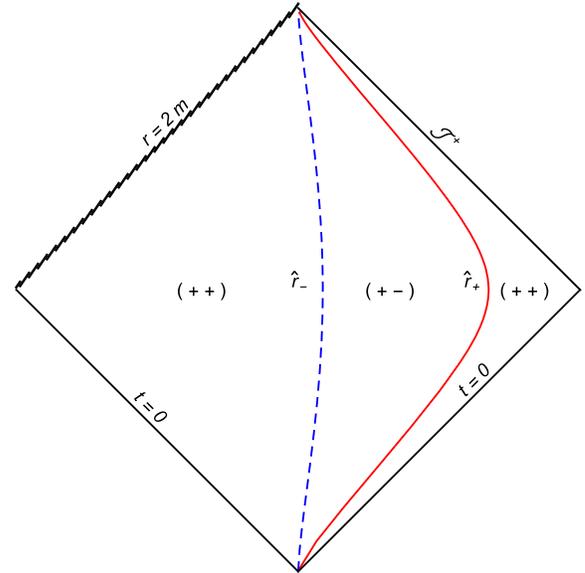

FIG. 12. The causal diagram for $a(t) = (t/t_0)$. The initial singularity is lightlike. If $t_0 > 8m$ the trapping horizons are as shown in this plot, being timelike everywhere. Here we have used $t_0 = 10m$, with $m = 1$. In such a case, the locus $r = 2m$ is singular

The scale factor $a(t) = (t/t_0)$ corresponds to the cosmological model of a universe filled by a fluid for which $p/\rho = -1/3$. Historically, the equation of state of such a form has been related to a fluid of cosmic strings [41,42]. However, with the advent of the accelerated expansion of the Universe, a plethora of dark energy models with $p/\rho < 0$ have been formulated. In particular, successful scalar field models imply in a relation $\omega = p/\rho$ which varies with the cosmological time and assumes negative values at late times, including the $\omega = -1/3$ as a particular situation.

The energy density, the pressure, and the energy flux are, respectively,

$$8\pi\rho = \frac{-8\pi p}{3} = \frac{3}{t^2 f(r)}, \qquad 8\pi|q| = \frac{2mt_0}{t^2} \frac{1}{r^2 f(r)}, \quad (55)$$

where $f(r)$ is given by Eq. (6). The curves for ρ, p, and for the ratio $(\rho + p)/2|q|$ as a function of the cosmological time, for fixed $r = 2.5m$, are shown in Fig. 13.

Here one has $n(t,r) = (\rho + p)/2|q| = r^2/(2mt_0)$, which depends only on the radial coordinate r, and is smaller than unity for small r. Since the constraint $\rho + p \geq 2|q|$ is not fulfilled, the energy conditions are violated at small scales. For $r \geq \sqrt{2mt_0}$ the NEC and the WEC are satisfied, but the SEC is not. In fact, the SEC is violated everywhere in the spacetime.

In the situation as in the case of Fig. 12, i.e., for $t_0 > 8m$, the horizons are formed at $t = 0$ with $\hat{r}_\pm(t) = (1 \pm \sqrt{1 - 8m/t_0})/(2t_0)$ and last forever. The NEC and the WEC are satisfied for all times along
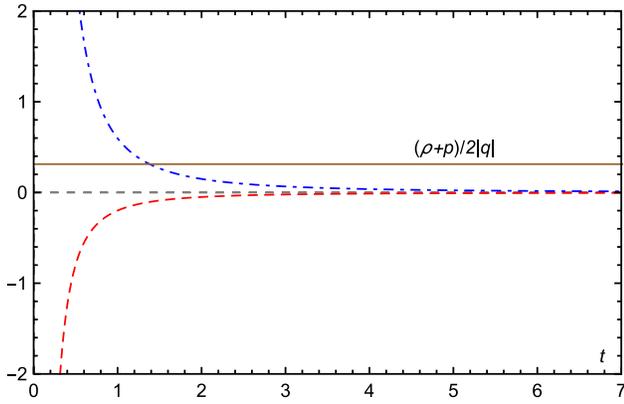
FIG. 13. The energy density, the pressure, and the ratio $(\rho + p)/2|q|$, from Eq. (55) with $r = 2.5m$, for the case $a(t) = t/t_0$, with $t_0 = 10m$ and $m = 1$.

$\hat{r}_+(t)$, but all the energy conditions are violated along $\hat{r}_-(t)$. See Appendix D for more details.

C. Solutions with bounded scale factor

1. Preliminaries

On the basis of the statement of Ref. [43] that a bound system either completely follows the cosmological expansion or is completely insensitive to it after some transient, it is reasonable to assume that, initially, the mass of the central object follows the expansion and grows with the cosmological scale factor $a(t)$, $M = ma(t)$, but that latter it stops to follow expansion and the mass increases in a different rate. These conditions justify the choice of a different function $a(t)$ to describe the mass function M, at least for late times.

Moreover, as already mentioned, an aim of the present work is to extract black-hole solutions from the Thakurta metric (2), and so the $r = 2m$ locus needs to be a nonsingular surface. In order to achieve such an objective, besides converging to a constant for large times, the study presented in Sec. IV elucidated that the scale factor $a(t)$ must display a sufficiently fast decaying derivative $\dot{a}(t)$.

Besides the physical interpretation of the matter under collapse, the important point here is that the choice of a bounded scale factor $a(t)$ bears the idea that the time evolution of the "local" object depart from the evolution of the Universe as a whole. In this instance, the function $M(t) = ma(t)$ describes the time evolution of the localized object independently of the expansion of the Universe which would be described by a different scale factor.

2. $a(t) = \tanh^{2/3}(t/t_0)$: Initial power law model with smooth transition to vacuum

With the last comments in mind, we try the function $a(t) = \tanh^{2/3}(t/t_0)$. This model simulates a dust dominated initial era, with $a(t) \sim (t/t_0)^{2/3}$, and a final phase with constant $a(t) = 1$.
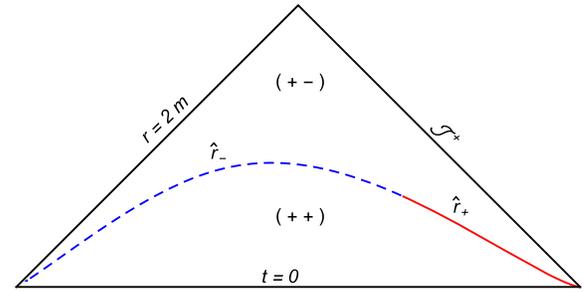

FIG. 14. The causal diagram for $a(t) = \tanh^{2/3}(t/t_0)$, with $t_0 = 1 = m$. The trapping horizons are spacelike everywhere, and the surface $r = 2m$ is nonsingular. Also there is an initial spacelike singularity at $t = 0$.

The scale factor $a(t) = \tanh^{2/3}(t/t_0)$ yields a spacetime whose incomplete causal diagram, for $t_0 = 1 = m$, is given in Fig. 14. The surface $r = 2m$ is nonsingular and the resulting spacetime is future geodesically incomplete along such a surface. Moreover, if we take $t_0 < 4m$—note that $t_0 = 2\tau$—then this spacetime can be extended and a possible extension is represented in Fig. 15. Taking into account that in the limit $t \to \infty$ these Thakurta models converge to a Schwarszchild geometry, and that the trapping horizons are everywhere spacelike, then the gluing is made from a regular region. Therefore the extension is made by joining a trapped Schwarszchild region, followed by a regular Schwarszchild region, and so on. A more detailed and rigorous argument on this point is presented in Appendix B, where we build Kruskal-like coordinates for the Thakurta spacetimes and discuss the conditions on its analytical continuation.

The background energy density, pressure, and energy flux in this case are, respectively,

$$8\pi\rho = \frac{16\text{csch}^2(2t/t_0)}{3t_0^2 f(r)}, \qquad 8\pi p = \frac{8\text{sech}^2(t/t_0)}{3t_0^2 f(r)},$$

$$8\pi|q| = \frac{4m}{3r^2 t_0} \frac{\text{sech}^2(t/t_0)}{\tanh^{5/3}(t/t_0)f(r)}, \tag{56}$$
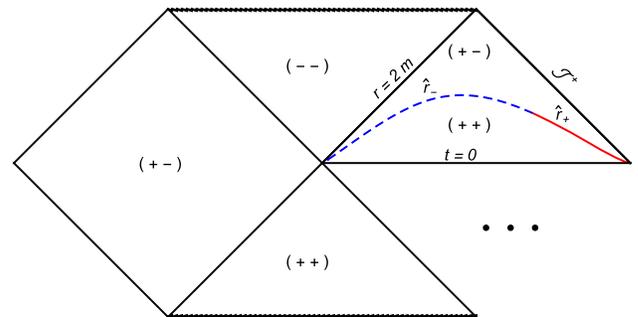

FIG. 15. A possible extended causal diagram for $a(t) = \tanh^{2/3}(t/t_0)$, with $t_0 = 1 = m$. The surface $r = 2m$ is nonsingular and corresponds to a black-hole horizon. The ellipses indicate that the diagram is to be continued.
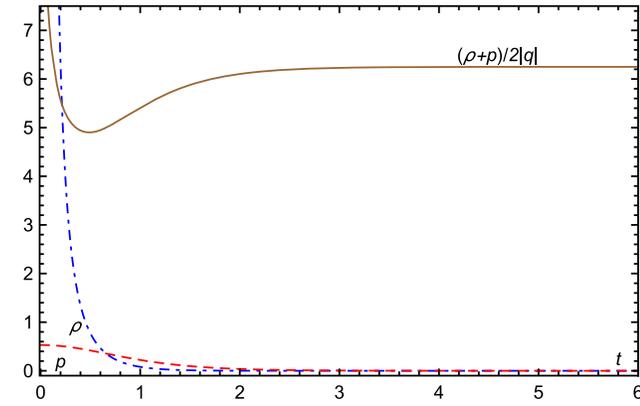
FIG. 16. The energy density, the pressure, and the ratio $(\rho + p)/2|q|$, for the case $a(t) = \tanh^{2/3}(t/t_0)$, with $t_0 = m$ and a fixed value of $r > 2m$ (here, $r = 2.5m$ and $m = 1$).

where $f(r)$ is given by Eq. (6). For small times it holds $a(t) \sim (t/t_0)^{2/3}$, and so the energy density approaches the cold dark matter cosmological model, $8\pi\rho \sim 4/(3t^2 f(r))$ but the pressure is constant with time in that regime, $8\pi p \sim 8/(3t_0^2 f(r))$. For large times both the energy density and pressure vanish, with the energy density going to zero faster than the pressure. The ratio p/ρ gives $2\sinh^2(t/t_0)$, which grows with e^{2t/t_0} at large times. This is shown in Fig. 16.

To check the energy conditions let us then take the ratio $(\rho + p)/2|q|$ from Eq. (15), which gives, $n(t,r) = \frac{r^2}{2mt_0}(1 + \coth^2(t/t_0))\tanh^{5/3}(t/t_0)$. For small times it results $n(t,r) \sim r^2/(2mt_0^{2/3}t^{1/3})$, while for large t it tends to $n(t,r) \to r^2/(mt_0)$. Hence, at initial times and fixed $r < \infty$ the constraint $(\rho + p) \geq 2|q|$ does not hold and the energy conditions are not satisfied. On the other hand, for large times and with fixed $r^2 > 2mt_0$ the energy flux is always smaller than the energy density and then the constraint $\rho + p \geq 2|q|$ is satisfied, which assures that the NEC is satisfied. Moreover, owing to the fact that in the present case one has $\rho + p > 0$, the WEC and the SEC are also satisfied for large times.

The analysis of the energy conditions and properties of the trapping horizons are presented in Appendix D.

3. $a(t) = \tanh(t/t_0)$: Cosmic strings type fluid model with smooth transition to vacuum

Let us now analyze a case with an initial singularity that is not spacelike and with bounded $a(t)$ at large times. This is the case for $a(t) = \tanh(t/t_0)$. At early times $t \to 0$ the scale factor goes as $a(t) = t/t_0$ and tends to unity for large times. The ratio between pressure and energy density for early times is $p/\rho = -1/3$, representing a fluid of cosmic strings [41,42]. This solution presents three possible structures depending on the value of t_0 that influence the behavior of the horizons. The analysis of this behavior is presented in Appendix A.
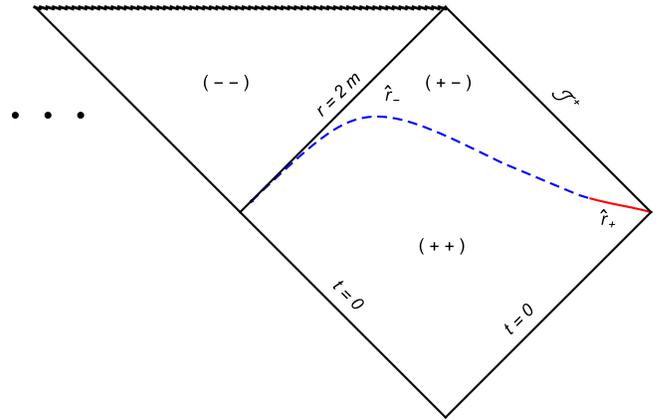

FIG. 17. The extended causal diagram for the case $a(t) = \tanh(t/t_0)$, with $t_0 = 3m$ and $m = 1$. The initial singularity is lightlike, and the surface $r = 2m$ is nonsingular and corresponds to a black-hole horizon. The trapping horizons $\hat{r}_-$ and $\hat{r}_+$ are spacelike for all times.

Considering $t_0 < 4m$ the horizons are spacelike at all times as showed in Fig. 17. For $4m < t_0 < 8m$ the horizon $\hat{r}_-$ is timelike at large times and the diagram is represented in Fig. 18. Also considering $t_0 > 8m$, represented in Fig. 19, the horizon $\hat{r}_-$ is timelike and both horizons exist at all times.

In the case $a(t) = \tanh(t/t_0)$, the energy density, the pressure, and the energy flux are given, respectively, by
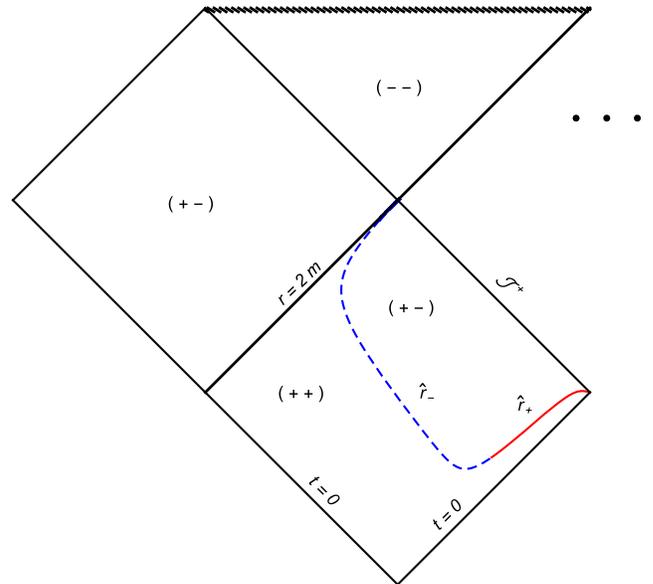

FIG. 18. The extended causal diagram for the case $a(t) = \tanh(t/t_0)$, with $t_0 = 6m$ and $m = 1$. The inner trapping horizon is timelike for late times, but it is spacelike in a small region of the spacetime at early times, close to the time the horizons are formed. The outer horizon is timelike for early times and becomes spacelike at late times. The initial singularity is lightlike, and the surface $r = 2m$ is nonsingular corresponding to a white-hole horizon.
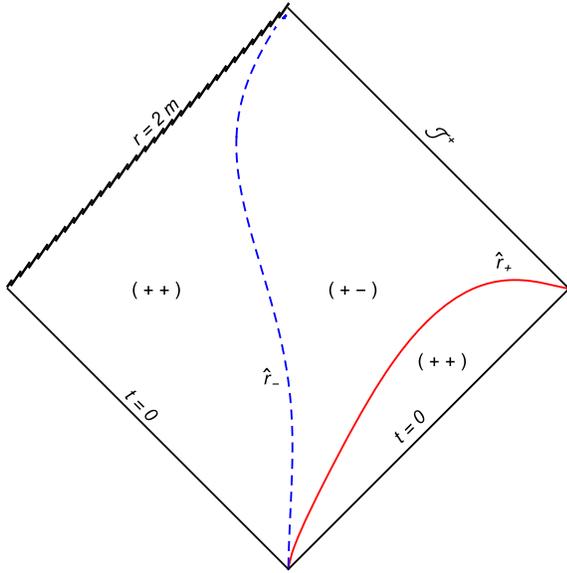
FIG. 19.   The causal diagram for the case $a(t) = \tanh(t/t_0)$, with $t_0 = 10m$ and $m = 1$. The inner horizon $\hat{r}_-$ is timelike, while the outer horizon $\hat{r}_+$ is timelike for early times and becomes spacelike at late times. The initial singularity is lightlike, and the surface $r = 2m$ is singular. Notice that the horizons exist since the beginning of time.

$$8\pi\rho = \frac{12\,\mathrm{csch}^2(2t/t_0)}{t_0^2 f(r)},$$

$$8\pi p = [2\cosh(2t/t_0) - 3]\frac{4\,\mathrm{csch}^2(2t/t_0)}{t_0^2 f(r)},$$

$$8\pi|q| = \frac{2m}{t_0}\frac{\mathrm{csch}^2(t/t_0)}{r^2 f(r)}, \tag{57}$$

where $f(r)$ is given by Eq. (6).

As seen in Figs. 20 and 21, this scale factor gives a fluid whose energy density and pressure diverge at $t = 0$ and vanish at $t \to \infty$. As in general for the Thakurta metric, the equation of state is such that $w = p/\rho$ depends on the
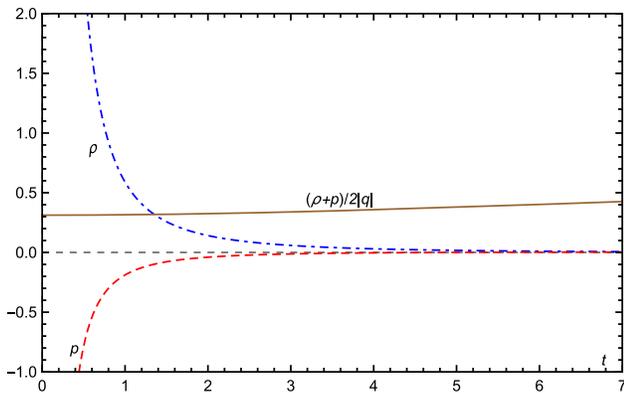

FIG. 20.   The energy density and the pressure from Eq. (57) for the case $a(t) = \tanh(t/t_0)$, with $t_0 = 10m$, $r = 2.5m$ and $m = 1$.
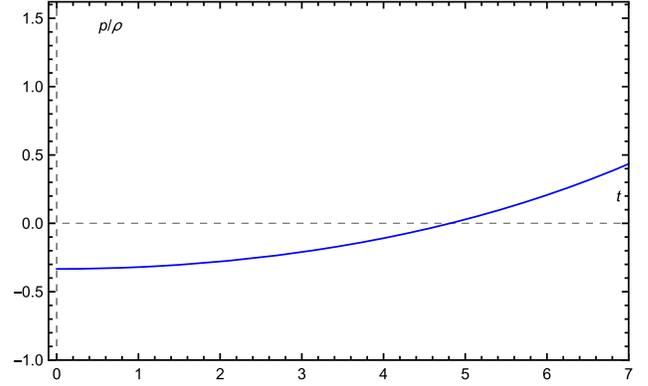

FIG. 21.   The ratio p/ρ in the case $a(t) = \tanh(t/t_0)$, with $t_0 = 10m$ and $m = 1$, as in Fig. 20.

cosmological time alone. Here it is $w(t) = -1 + 2\cosh(2t/2t_0)/3$. Function $w(t)$ assumes the value $p/\rho = -1/3$ at $t \to 0$, the equation of state for a fluid of cosmic strings [41,42]. The pressure grows to positive values and decays to zero in a rate slower than the energy density, and then the ratio $w(t)$ changes signs and assumes large values for large times, even though the fluid quantities are vanishingly small.

The ratio $(\rho + p)/2|q|$ starts with the value $r^2/(2mt_0)$ at $t = 0$ and reaches the value $r^2/(mt_0)$ at $t \to \infty$. Hence, the (NEC, WEC and SEC) energy conditions are violated for sufficiently small radial coordinate, but they are all satisfied for sufficiently large values of r. This implies that the energy conditions tend to be violated along the $\hat{r}_-(t)$ branches of the trapping horizons, and are satisfied along the $\hat{r}_+(t)$ branch. In Appendix D we perform a more detailed analysis on such a subject.

4. Truncated scale factor

Some of the models with unbounded scale factor can easily be modified to describe a spacetime without a singularity at $r = 2m$. Considering that the accretion of matter/energy into the central object eventually ceases because the whole matter of the surroundings has already been exhausted, we may take a different scale factor $a(t)$ after a given sufficiently long time T. Notice that a nonsingular surface $r = 2m$ can be formed if we choose $\dot{a}(t)$ to vanish faster than $\exp(-t/2m)$. The simplest choice is to take $a(t) = \text{constant}$ for $t > T$.

For instance, in the case of dust matter studied in Sec. V B 3 we may take

$$a(t) = \begin{cases} (t/t_0)^{2/3}, & t \le T, \\ (T/t_0)^{2/3}, & t > T, \end{cases} \tag{58}$$

where T is an arbitrary timescale. In this case, the mass function $M(t) = ma(t)$ initially grows by accretion of dust fluid (cold dark matter) at the same rate as the background expands, but suddenly stops growing at time T.
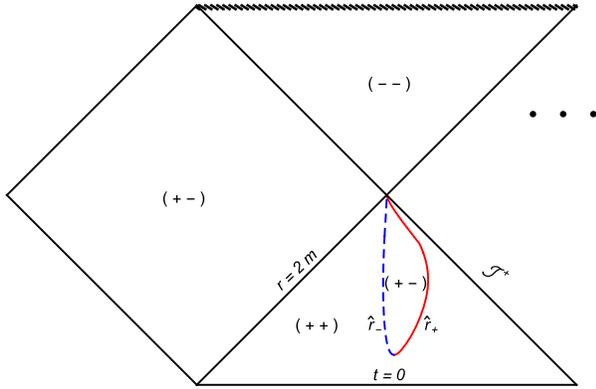
FIG. 22. The extended causal diagram in the case the scale factor is truncated as $a(t) = (t/t_0)^{2/3}$ for $t \leq T$, and $a(t) = (T/t_0)^{2/3} = $ constant for $t > T$. Here we have chosen $T = 50m$, $t_0 = m$, and $m = 1$. The initial singularity $t = 0$ is spacelike. The locus $r = 2m$ is nonsingular and corresponds to a white-hole horizon.

This parameter T is chosen as the approximate cosmological time when the evolution of local object separates from the universal expansion. Such a time scale may be thought of as the time when the accretion of matter by the object becomes negligible.

The final spacetime is a white hole. In fact, the causal diagram is similar to what is presented in Fig. 8, but now the locus $r = 2m$ is nonsingular, the resulting geometry is geodesically incomplete and the spacetime can be extended as shown in Fig. 22, where the extension is made by attaching a regular region, followed by a trapped region, into the antitrapped region.

A second interesting example where the scale factor may be truncated after a given time is the case considered in Sec. V B 5. The scale factor is of the form

$$a(t) = \begin{cases} t/t_0, & t \leq T, \\ T/t_0, & t > T, \end{cases} \tag{59}$$

where T is an arbitrary timescale. The corresponding conformal diagram is shown in Fig. 23.

Is is also easy to obtain a black-hole type solution in the case of $a(t) = \tanh(t/t_0)$, with $t_0 = 10m$, studied above by truncating the scale factor in order to make it tend to a constant faster enough. Then, by choosing

$$a(t) = \begin{cases} \tanh(t/t_0), & t \leq T, \\ \tanh(T/t_0), & t > T, \end{cases} \tag{60}$$

where $a(t)$ is a constant for $t > t_0$, an extension of the spacetime represented by Fig. 19 can be found. With this, the locus $r = 2m$, or $R = 2ma(t)$, is asymptotically a nonsingular lightlike surface. The final state is a white hole. Figure 24 shows a possible analytical continuation of the spacetime corresponding to this truncated scale factor.
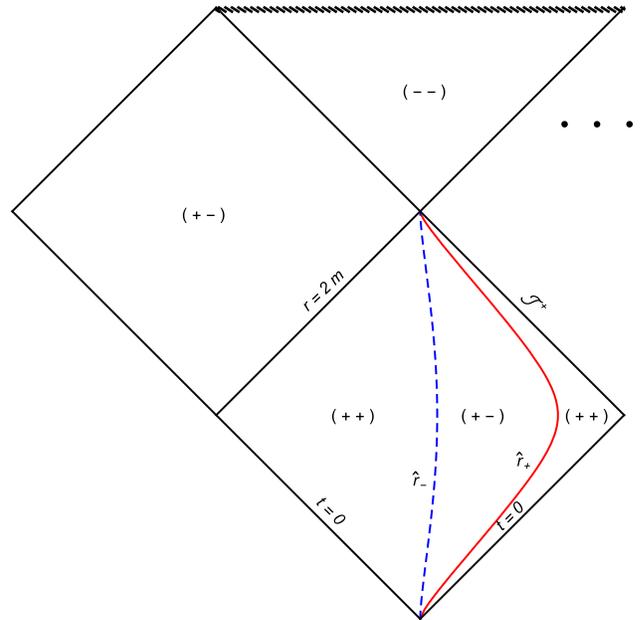

FIG. 23. A possible extension in the case $a(t) = t/t_0$, for $T \leq T$, and $a(t) = T/t_0$, for $t > T$. Here we have chosen $T = t_0 = 10m$, and $m = 1$. In such a case the surface $r = 2m$ is nonsingular and corresponds to a white-hole horizon.

Let us stress that the models analyzed in this subsection should be considered as first approximations to describe the *local* evolution of the spacetime, with the term *local* meaning the spacetime region close to central object.
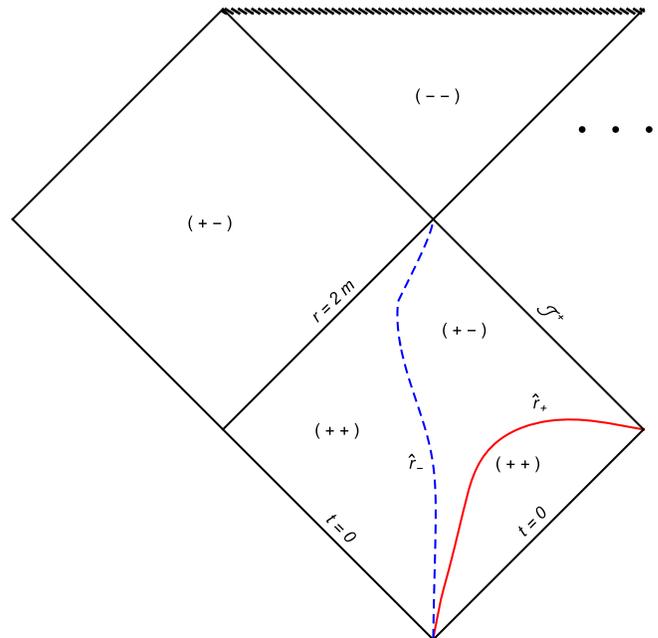

FIG. 24. A possible extension for the case $a(t) = \tanh(t/t_0)$ for $t < T$ and $a(t) = \tanh(T/t_0)$ for $t \geq T$, with $T = 50m$, $t_0 = 10m$, and $m = 1$. The surface $r = 2m$ is nonsingular and corresponds to a white-hole horizon.

In fact, the truncation process causes an abrupt change in the spacetime evolution, and may introduce surface layers which could spoil the physical properties of the spacetime. The alternative to avoid such layers is to replace the constant a for $t > T$ by a function $a_2(t)$ which falls off with t in a rate such that $0 < \dot{a}_2(t) < e^{-t/4m}$, and to try a smooth match at $t = T$. Furthermore, the conditions $a(T) = a_2(T)$, $\dot{a}(T) = \dot{a}_2(T)$, and $\ddot{a}(T) = \ddot{a}_2(T)$ assure the continuity of the energy density, energy flux, and pressure at $t = T$. Then, a matching hypersurface of class C^2 is enough to avoid introducing surface layers. Such a construction does not change substantially the global causal structure of the spacetime, in the sense that the trapping horizons keep the asymptotic behavior and the surface $r = 2m$ is regular at $t \to \infty$, as in Figs. 22, 23, and 24, and leads to solutions with no shells/surface layers. The resulting $a_2(t)$ functions are given by cumbersome formulas and then we do not preset them here.

A possible issue remains in the case $a(t) = (t/t_0)^{2/3}$, because in this case the dust character of the fluid is broken. The C^2 matching inevitably introduces a nonzero pressure for $t > T$, i.e., nevertheless continuous at $t = T$, the pressure is zero for $t \leq T$ but it would not be zero for $t > T$ anymore. In order to fix the pressure to zero also in the region $t > T$, a surface layer must be present at $t = T$, and so the curvature scalar would acquire δ function terms. Such a situation is of little interest for the present analysis.

D. Further considerations

Many other examples can be constructed for different choices of $a(t)$, however they will present essentially the same causal structure. This is due to the fact that the causal structure is determined by the asymptotic behavior of the chosen scale factor $a(t)$ at two limits, namely, $t \to 0$ and $t \to \infty$. Therefore, we can craft any of the possible causal structures showed here, and still other ones that combine the possible behaviors of the big-bang singularity, the asymptotic character of the trapping horizons and the properties of the $r = 2m$ surface and its continuation beyond the horizon (if it is nonsingular) by building functions $a(t)$ with the required properties at those two limits.

VI. CONCLUSION

In this paper we performed a thorough study of the spacetimes built by a conformal transformation of the Schwarszchild metric in Schwarszchild coordinates, using a time-dependent scalar factor $a(t)$. We demonstrated that for unbounded scale factors $a(t)$, the resulting models do not describe black holes, but inhomogeneous expanding universes presenting a regular region with a finite lifespan or even spacetimes with a null singularity at a finite proper time in the future.

In order to obtain black-holes spacetimes, we had to resort for bounded scale factors, with a rapidly vanishing time derivative $\dot{a} \sim e^{-t/\tau}$. For instance, in the models with $a(t) = \tanh(t/t_0)$ the time derivative of the scale factor goes as $\dot{a} \sim e^{-2t/t_0}$. The properties of these models, even with similar functional forms, strongly depend on the value of τ. We have found that

(1) For $\tau > 4m$, the spacetime has a future null singularity and is not extensible;
(2) For $2m < \tau < 4m$, the spacetime presents a white-hole horizon at $r = 2m$;
(3) For $\tau < 2m$, the spacetime presents a black-hole event horizon at $r = 2m$.

The strong dependence of the causal structure on the asymptotic form of the scale function $a(t)$ is reminiscent of the cosmological black-hole solutions based on the McVittie metric, that can also represent white holes depending on the chosen parameters, as recently shown in Refs. [20,21]. The important difference here is that black-hole models only suffer cosmological expansion during a finite time scale given by the parameter τ, being essentially static for large times. This behavior may seem unphysical at first glance, but it can be thought of as a decoupling model of an initially bound system that, after a transient, decouples from the cosmological expansion, similar to the behavior of the classical atom studied in Ref. [43]. Therefore, this can be an interesting model for dynamical, accreting black holes, that after the accretion time decouples from the cosmological expansion and ceases to accrete, and that at late times lives in an effectively static and empty bubble.

This analysis leads us to realize how subtle the interpretation of apparently simple solutions of general relativity may be and provides examples of black holes and white holes with time-dependent mass and dynamical horizons. These results indicate that this construction of dynamical solutions from static ones can be used for other classes of black-hole solutions, as Thakurta's original attempt using Kerr line element. It is important to remark that this method of construction using a time-dependent conformal factor is dependent on the choice of the coordinates in the original metric. For example, in the case of Schwarszchild metric, a different choice of coordinates leads to the Sultana-Dyer construction [31].

Finally, we wonder that this method of building dynamical black holes from static ones may be employed to produce new solutions in a number of applications in black-hole physics, such as the AdS/CFT correspondence, black-hole thermodynamics and properties of general relativity in the strong field regime.

ACKNOWLEDGMENTS

APPENDIX A: ASYMPTOTIC BEHAVIOR OF THE TRAPPING HORIZONS

In order to determine the character of the horizons hypersurfaces we investigate the character of the normal vector $n_\mu = \partial_\mu \hat{r}_\pm$. We consider only cases where $\dot{a} \to 0$ as $t \to \infty$. In the cases where $\dot{a} \nrightarrow 0$ the horizons have a finite span in the $R \times t$ subspace and do not exist for sufficiently large times. The case $\dot{a}$ tends to a nonzero constant as $t \to \infty$ requires a separated study. The hypothesis $\dot{a} \to 0$ allows us to greatly simplify the expressions for the horizons by means of series expansions in terms of $\dot{a}$. Equation (26) can be approximated by

$$\hat{r}_+ = \frac{1}{\dot{a}} + \mathcal{O}(\dot{a}), \tag{A1}$$

$$\hat{r}_- = 2m(1 + 2m\dot{a}) + \mathcal{O}(\dot{a}^2). \tag{A2}$$

Therefore, the normal vectors to the trapping horizons $\hat{r}_\pm$ are given respectively by

$$n^{(+)} = \frac{\ddot{a}}{\dot{a}^2} dt + dr, \tag{A3}$$

$$n^{(-)} = -4m^2 \ddot{a} dt + dr. \tag{A4}$$

Taking the (squared) norm of $n^{(-)}$, for the inner horizon $\hat{r}_-$, we get

$$\begin{aligned}
|n^{(-)}|^2 &= -\frac{(4m^2)^2 \ddot{a}^2}{f[\hat{r}_-(t)])} + a^{-2} f[\hat{r}_-(t)] \\
&= -\frac{(4m^2)^2 \ddot{a}^2}{2m\dot{a}} + \frac{2m\dot{a}}{a^2},
\end{aligned} \tag{A5}$$

where we used the approximation

$$f[\hat{r}_-(t)] \approx 2m\dot{a}. \tag{A6}$$

Similarly, for the outer horizon $\hat{r}_+$ it follows

$$\begin{aligned}
|n^{(+)}|^2 &= -\frac{1}{1 - 2m\dot{a}} \frac{\ddot{a}^2}{\dot{a}^4} + a^{-2}(1 - 2m\dot{a}) \\
&= (1 + \mathcal{O}(\dot{a})) \left(\frac{1}{a^2} - \frac{\ddot{a}^2}{\dot{a}^4} \right),
\end{aligned} \tag{A7}$$

where the approximation

$$f[\hat{r}_+(t)] \approx 1 - 2m\dot{a}, \tag{A8}$$

was used.

With Eqs. (A5) and (A7) at hand, in order to determine the asymptotic character of the trapping horizons, we only need to determine the sign of the normal to the horizon surfaces for a given asymptotic behavior of the scale factor $a(t)$.

For scale factors of the type $a(t) \sim t^\alpha$, with $0 < \alpha < 1$, one has $\frac{\ddot{a}^2}{\dot{a}^4} \sim 1$, $\frac{\ddot{a}^2}{\dot{a}^2} \sim t^{-2}$, and $\frac{1}{a^2} \sim t^{-2\alpha}$. Applying this result to Eq. (A5) we obtain $|n^{(-)}|^2 > 0$ for large t. Therefore,

(1) $\hat{r}_-$ is timelike for large t if $0 < \alpha < 1$.

On the other hand, still for power law scale factors with $a(t) \sim t^\alpha$, the nature of the outer horizon depends upon α. From Eq. (A7) we obtain that

(1) $\hat{r}_+$ is timelike for large t if $\alpha > 1/2$,
(2) $\hat{r}_+$ is spacelike for large t if $\alpha < 1/2$.

In the case of models with a nonsingular surface at $r = 2m$, typically, the scale factor is such that $\dot{a} \sim e^{-t/\tau}$. With no loss of generality, we can set $a_\infty = 1$, since we can always achieve that by a rescaling $r \to \frac{r}{a_\infty}$, $m \to \frac{m}{a_\infty}$. Using Eqs. (A5) and (A7), it can be shown that for large times $\hat{r}_-$ and $\hat{r}_+$ behave as follows:

(1) $\hat{r}_-$ is spacelike if $\tau < 2m$,
(2) $\hat{r}_-$ is timelike if $\tau > 2m$,
(3) $\hat{r}_+$ is always spacelike.

APPENDIX B: THE NATURE OF THE HORIZON AT $r = 2m$

As seen above there are cases where the surface at $r = 2m$ is a null horizon and the metric at that locus has the Schwarzschild form. In order to build an analytical continuation, we have to determine the kind of horizon it is. Since the metric is conformal to Schwarzschild, we can use Kruskal-like coordinates in order to extend it. Let U and V be such coordinates, defined by

$$\begin{aligned}
U &= \exp\left(\frac{\eta + r^*}{2m}\right), \\
V &= -\exp\left(\frac{-\eta + r^*}{2m}\right),
\end{aligned} \tag{B1}$$

so that the metric (40) can be cast in the form

$$ds^2 = a^2(\eta) \frac{e^{-r/2m}}{r} (-dU dV + \cdots), \tag{B2}$$

which is well behaved at $r = 2m$, that is given by $V = 0$ in (U, V) coordinates. The null expansions at $r = 2m$ are

$$\begin{aligned}
\Theta_+|_{r=2m} &= V, \\
\Theta_-|_{r=2m} &= U.
\end{aligned} \tag{B3}$$

Note that the null surface $r = 2m$ is also a trapping horizon since $\Theta_+ = 0$ there. Since $\Theta_+ > 0$ in the region covered by (t, r) coordinates with $r > 2m$, by continuity it follows that $\Theta_+ < 0$ for $r < 2m$. This implies that the surface $r = 2m$ of the Thakurta model should be identified to the U axis of the half of a Schwarzschild spacetime defined by $V < 0$.

In order to determine to which quadrant of the Schwarzschild maximal extension we can continue the Thakurta nonsingular models, we have to analyze the sign of the expansion of ingoing rays as they reach the horizon. Using (t, r) coordinates again, we obtain

$$\Theta_- = \frac{2}{ar} k^\mu_{(-)} \nabla_\mu(ar) = \frac{2}{r} [\dot{a}r - f(r)], \qquad (B4)$$

which, evaluated for $r = r_-(t)$ and large t, gives

$$\Theta_- \approx \frac{1}{m}(2m\dot{a} - e^{-t/2m}). \qquad (B5)$$

Hence, assuming $\dot{a} \sim e^{-t/\tau}$, Eq. (B5) implies in
(1) $\Theta_- < 0$ if $\tau < 2m$,
(2) $\Theta_- > 0$ if $\tau > 2m$,
which are the same conditions found for the asymptotic character of the inner trapping horizon $\hat{r}_-$ in Appendix A.

In the case where $\Theta_- < 0$ as $r_- \to 2m$, the horizon at $r = 2m$ is the boundary of a regular region, and hence the analytical continuation must be into a trapped region of the Schwarzschild spacetime, corresponding to the region II $(V < 0, U < 0)$ of its maximal extension.

In the case where $\Theta_- > 0$ as $r_- \to 2m$, the horizon at $r = 2m$ is the boundary of an antitrapped region, and hence the analytical continuation must be into a regular region of the Schwarzschild spacetime, corresponding to the region I $(V < 0, U > 0)$ of its maximal extension.

This argument justifies the analytical continuations of Thakurta spacetimes presented in Figs. 15, 17, 18, 22, 23, and 24.

APPENDIX C: GEODESIC COMPLETENESS CONSIDERING SUBLEADING TERMS

Here we extend the analysis of the geodesic completeness made in Sec. III C including the contribution of subleading terms.

We start defining $\Delta(t) = r_- - 2m$ so that Eq. (28) can be written in terms of $\Delta(t)$ as

$$t'' = \left[\frac{1}{2ma}\left(1 + \frac{r_- + 2m}{r_-^2}\Delta(t)\right) - \frac{\dot{a}}{a}\right]t'^2, \qquad (C1)$$

which gives, instead of Eq. (31),

$$\ln t' = \frac{\eta}{2m} - \ln a + \frac{1}{2m}\int^t \frac{(r_-(s) + 2m)}{a(s)r_-(s)}\Delta(s)ds + c_1, \qquad (C2)$$

where c_1 is an arbitrary integration constant. Let us stress that Eq. (C2) is an exact relation. Therefore, instead of Eq. (32), we find for the affine parameter

$$\Delta\lambda = c_2 \int_{t_0}^t e^{-\frac{\eta(u)}{2m}}a(u)e^{-J(u)}du \qquad (C3)$$

where c_2 is another integration constant and we defined

$$J(u) = \frac{1}{2m}\int_{t_0}^u \frac{(r_-(s) + 2m)}{a(s)r_-(s)}\Delta(s)ds. \qquad (C4)$$

The crucial difference between Eq. (C3) and Eq. (32) is the presence of the second exponential term in the integrand, $e^{-J(u)}$. The first exponential term, $e^{-\frac{\eta(u)}{2m}}$, is essentially the same as in Eq. (32) (taking $K = 1/2m$ they become identical) and then, to complete the analysis including subleading terms, just the behavior of the second exponential term as $t \to \infty$ must be studied here.

We first notice that, since $r_-(t) > 2m$, $\forall\, t > 0$, it follows that $\Delta(t) \geq 0$ and the ratio $(r_- + 2m)/r_-$ is bounded, more precisely one has $1 < \frac{r_- + 2m}{r_-} < 2$, $\forall\, t > 0$. Therefore, it suffices to study the properties of the simpler expression

$$I(u) = \exp\left(\frac{1}{2m}\int_{t_0}^u \frac{\Delta(s)}{a(s)}ds\right). \qquad (C5)$$

Now it is convenient to consider separately the two possibilities,
(1) $\lim_{t\to\infty}\Delta(t) > 0$, which corresponds to η bounded from above.
(2) $\lim_{t\to\infty}\Delta(t) = 0$, which corresponds to η unbounded from above.

In the first case, if Δ tends to a finite positive value, then, for any s in the time interval considered (t_0, u), there exist constants Δ_b, Δ_a such that $0 < \Delta_b \leq \Delta(s) \leq \Delta_a$, implying in

$$[\eta(u) - \eta(t_0)]\Delta_b \leq \int_{t_0}^u \frac{\Delta(s)}{a(s)}ds \leq [\eta(u) - \eta(t_0)]\Delta_a. \qquad (C6)$$

Taking the limit $u \to \infty$ and applying to $I(u)$ we finally obtain

$$0 < \exp\left[-\frac{\Delta_a}{2m}(\eta_\infty - \eta(t_0))\right] < \lim_{u\to\infty}I(u)$$

$$< \exp\left[-\frac{\Delta_b}{2m}(\eta_\infty - \eta(t_0))\right], \qquad (C7)$$

which demonstrates that $I(u)$ is bounded by two strictly positive constant values, and so the subleading terms give no relevant contribution to the convergence properties of $\Delta\lambda$. This fact guarantees that the study of Eq. (32) as the criterion for convergence performed in Sec. III C is a strong result.

Now we examine the case where $\Delta(t) \to 0$ as $t \to \infty$. As in Sec. III C we take a linear scale factor $a(t) = a_0 t$, a_0 being a constant parameter. In this case we have to review the argument since there is no $\Delta_b > 0$ that bounds $\Delta(t)$ from below. However, Eq. (29) can be expressed in terms of Δ to find

$$e^{1+\frac{\Delta(t)}{2m}}\Delta(t) = \left(\frac{t}{t_0}\right)^{-\frac{1}{2ma_0}}. \qquad (C8)$$

Replacing the last result into Eq. (C5) yields

$$I(u) = \exp\left(\frac{1}{2m}\int_{t_0}^{u} e^{1+\frac{\Delta(s)}{2m}} \frac{t_0^{1/2ma_0}}{s^{1+1/2ma_0}} ds\right), \qquad (C9)$$

which is convergent in the limit $u \to \infty$. Therefore, taking into account the bounded character of $I(u)$, $0 < \lim_{u\to\infty} I(u) < c_3$ for some constant $c_3 > 0$, the convergence of $\Delta\lambda$ is determined by the first exponential term $e^{-\eta/2m}$ as in Eq. (32), recovering the results obtained in Sec. III C.

APPENDIX D: THE ENERGY CONDITIONS AND THE NATURE OF THE TRAPPING HORIZONS

Here we investigate in some detail the character of the horizons within the models presented in Sec. V.

A trapping horizon h is defined from the condition $\Theta_-\big|_h = 0$. Correspondingly (following Ref. [22]), h is said to be a past (future) trapping horizon if $\Theta_+\big|_h > 0$ ($\Theta_+\big|_h < 0$). The horizon is outer (inner) if $\mathcal{L}_+\Theta_-\big|_h < 0$ ($\mathcal{L}_+\Theta_-\big|_h > 0$), where $\mathcal{L}_+$ stands for the Lie derivative along the outgoing null geodesic lines.

The present analysis is based on the studies of Refs. [22,39], which present theorems that relate the chronological character of the trapping horizons to the null energy condition. Here, for the sake of simplicity, we stick to the statement given in Ref. [22], though it is weaker in general than the one presented in [39]. In the present models, however, since metric and horizons are spherically symmetric, they are equivalent. The statement is

Theorem I.—If the null energy condition holds, then an outer (inner) trapping horizon is spacelike (timelike), and a trapping horizon is null if and only if, additionally, the internal shear and normal energy density (energy flux) vanish.

1. The case of Sec. V B 2

In the situation of Fig. 6, the horizons are formed at $t = t_i \simeq 0.31$, with values $\hat{r}_\pm(t_i) = 4.0$ and disappear at $t = t_f \simeq 62.82$ also with values $\hat{r}_\pm(t_i) = 4.0$. We have calculated the ratio $n(t, r)$ [see Eq. (15)] for $r = \hat{r}_\pm(t)$ and checked the energy conditions along both horizons.

(1) Along $\hat{r}_+(t)$: The NEC, the WEC and the SEC are satisfied since it is formed, but all the energy conditions are violated along $\hat{r}_+(t)$ for times close to t_f. In particular, the NEC is satisfied up to $t_c \simeq 38.73$. Close to the initial time $t_i \simeq 0.31$ one has $\mathcal{L}_+\Theta_- < 0$, but it becomes positive for times greater than $t_1 \simeq 0.44$. Hence, given that $\Theta_+ > 0$ and $q(t, r_+(t)) \neq 0$, according to Theorem I, $\hat{r}_+(t)$ is a past outer spacelike horizon in the region $t \in [t_i, 0.44]$. For later times, one has $\mathcal{L}_+\Theta_- > 0$ [$\hat{r}_+(t)$ changes character from outer to inner] and so it becomes a past inner timelike (Lorentzian) horizon in that region (i.e., for $t \in [t_1 \simeq 0.44, t_c \simeq 38.73]$), as predicted from the mentioned theorem. For times later than $t_c \simeq 38.73$ the NEC is not fulfilled in $\hat{r}_+(t)$ and Theorem I does not apply. But, we verify that it changes back to spacelike character close to $t = t_f$. More precisely, it is an outer spacelike horizon in the interval $t \in [t_c, t_f]$.

(2) Along $\hat{r}_-(t)$: The energy conditions are satisfied just very close to the initial t_i, and are all violated for later times ($t > t_2 \simeq 0.35$ with the data of Fig. 6). Given that $\Theta_+ > 0$, $\mathcal{L}_+\Theta_- < 0$, and $q \neq 0$, it follows that $\hat{r}_-(t)$ is a past outer spacelike horizon in the region $t \in [0.31, 0.35]$. For later times the NEC is violated and so Theorem I does not apply. However, it can be shown that $\hat{r}_-(t)$ is a past outer timelike horizon for intermediate times, in the interval $t \in [0.35, 58.99]$, changing back to inner spacelike character close to t_f, in the interval $t \in [59.0, 62.82]$.

2. The case of Sec. V B 3

In the case of dust matter, the ratio $n(t, r_+(t))$ [see Eq. (15)], is larger than unity for all times after the horizon formation along $r = \hat{r}_+(t)$, while $n(t, \hat{r}_-(t))$ is larger than unity just for very early times after horizons formation. In the situation of Fig. 8, the horizons are formed at $t = t_i = 4096m^3/27t_0^2 \simeq 151.70$, with values $\hat{r}_\pm(t_i) = 4.0$ and last forever. In fact, $\hat{r}_+(t) \to 3t_0(t/t_0)^{1/3}/2$ and $\hat{r}_-(t)$ tends to $2m$ as $t \to \infty$.

(1) Along $\hat{r}_+(t)$: The NEC, the WEC and the SEC are satisfied all along $\hat{r}_+(t)$. The Lie derivative $\mathcal{L}_+\Theta_-\big|_{\hat{r}_+(t)}$ changes sign at $t_c = 216.0$. Close to t_i, more precisely, in the interval $[t_i, t_c]$, the condition $\mathcal{L}_+\Theta_- < 0$ holds (besides $\Theta_+ > 0$ and $q \neq 0$) and then $\hat{r}_+(t)$ is a past outer spacelike horizon in that region. For later times, $\mathcal{L}_+\Theta_- > 0$ and so, in the

interval $t \in [t_c, \infty)$, the $\hat{r}_+(t)$ branch changes character to a past inner timelike horizon, as predicted from Theorem I.

(2) Along $\hat{r}_-(t)$: The energy conditions are satisfied just close to the initial (t_i), and are all violated for late times $(t > t_m \simeq 172.47$ with the data of Fig. 6). Given that $\Theta_+ > 0$, $\mathcal{L}_+\Theta_- < 0$, and $q \neq 0$, $\hat{r}_-(t)$ is a past outer spacelike horizons in the region $t \in [t_i, t_m]$. For times larger than t_m, the NEC is violated and Theorem I does not apply, but it can be shown that $\hat{r}_-(t)$ is a past outer timelike horizon for all times after t_c.

3. The case of Sec. V B 4

In the case of stiff matter, the ratio $n(t, r_+(t))$, along $r = \hat{r}_+(t)$, is larger than unity for all times after the horizon formation, while $n(t, \hat{r}_-(t))$ is larger than unity just at early times after horizons formation. In the situation of Fig. 10, the horizons are formed a t $t = t_i \simeq 4.35$, with values $\hat{r}_\pm(t_i) = 4.0$ and last forever. In the limit of very large times $\hat{r}_+(t)$ goes as $3t_0(t/t_0)^{2/3}/2$ while $r_-(t) \to 2m$.

(1) Along $\hat{r}_+(t)$: The NEC and the WEC are satisfied for all times on $\hat{r}_+(t)$ since it is formed, but we can show that the SEC is not satisfied along it. Once the NEC is satisfied and, moreover, $\Theta_+ > 0$, $\mathcal{L}_+\Theta_- < 0$, and $q \neq 0$ all along $\hat{r}_+(t)$, according to Theorem I, it is a past outer spacelike horizon (see Fig. 10).

(2) Along $\hat{r}_-(t)$: The NEC and the WEC are satisfied at the beginning $(t \gtrsim t_i)$, but all energy conditions are violated for times larger that $t_c \simeq 6.70$. As in the case of the last section, at times close to t_i one has $\mathcal{L}_+\Theta_- < 0$ and $q \neq 0$, and since the NEC is satisfied along $\hat{r}_-(t)$, Theorem I implies it is a past outer spacelike horizon in the region $t \in [4, 6.70]$. For later times, the NEC is violated and so the hypothesis of the above mentioned theorem is not fulfilled, but it is verified that $\hat{r}_-(t)$ is a past outer timelike horizon in that region.

4. The case of Sec. V B 5

In this case, $a(t) = t/t_0$, if $t_0 \geq 8m$ the trapping horizons are formed at $t = 0$ and persist for all times with constant values. In the particular case of Fig. 12, where $t_0 = 10m$, $m = 1$, the values are $\hat{r}_+(t) \simeq 7.24$ and $\hat{r}_-(t) \simeq 2.76$.

(1) Along $\hat{r}_+(t)$: The NEC is satisfied for all times, and, moreover, considering that $\Theta_+ > 0$, $\mathcal{L}_+\Theta_- > 0$, and $q \neq 0$ at all times on $\hat{r}_+(t)$. Thus, according to the relevant theorem one has that it is a past inner timelike horizon (see Fig. 12).

(2) Along $\hat{r}_-(t)$: The NEC is violated at all times along this branch of the trapping horizon and the predictions of Theorem I cannot be applied. However, since one has $\Theta_+ = 0$ and $\mathcal{L}_+\Theta_- < 0$ it results that $\hat{r}_-(t)$ is a past outer horizon, and it can also be shown that it is everywhere timelike.

5. The case of Sec. V C 2

In the situation of Fig. 14, the horizons $\hat{r}_\pm(t)$ are formed at $t \simeq 1.498$ with values $\hat{r}_\pm = 4.0$, and last forever. Their asymptotic values for large times are $\hat{r}_-(t) = 2m$ and $\hat{r}_+(t) = 3t_0 e^{2t/t_0}/2$. For such a case, we have shown that $n(t, \hat{r}_+(t)) \geq 1$, and that the NEC, the WEC and the SEC are obeyed all along $r_+(t)$. The same holds along $\hat{r}_-(t)$.

(1) Along $\hat{r}_+(t)$: The NEC is satisfied for all times, and, moreover, considering that $\Theta_+ > 0$, $\mathcal{L}_+\Theta_- < 0$, and $q \geq 0$ at all times on $\hat{r}_+(t)$, according to Theorem I it is a past outer spacelike horizon.

(2) Along $\hat{r}_-(t)$: The NEC holds at all times along this branch of the trapping horizon and the predictions of the mentioned theorem, together with the conditions $\mathcal{L}_+\Theta_- < 0$ and $q \neq 0$ on $\hat{r}_-(t)$, imply it is a past outer spacelike horizon (see Fig. 14).

6. The cases of Sec. V C 3

For $a(t) = \tanh(t/t_0)$ it is convenient to split the analysis into three different classes according to the values of t_0: (a) $t_0 < 4m$; (b) $4m < t_0 < 8m$; and (c) $t_0 > 8m$.

a. The case $t_0 < 4m$

In the situation of Fig. 17, with $t_0 = 3m$, $m = 1$, the horizons are formed at $t_i \simeq 3.22$ with values $\hat{r}_\pm(t_i) = 4.0$ and last forever. In the limit $t \to \infty$, $\hat{r}_+(t)$ tends to $t_0 e^{2t/t_0}$ while $\hat{r}_-(t)$ tends to $2m$.

(1) Along $\hat{r}_+(t)$: The NEC is satisfied for all times, and, moreover, considering that $q \neq 0$ and $\mathcal{L}_+\Theta_- < 0$ at all times on $\hat{r}_+(t)$, according to the relevant theorem it is a past outer spacelike horizon.

(2) Along $\hat{r}_-(t)$: The NEC holds at all times along this branch of the trapping horizon and the predictions Theorem I, together with the conditions $q \neq 0$ and $\mathcal{L}_+\Theta_- < 0$ on $\hat{r}_-(t)$, which are fulfilled at all times on $\hat{r}_-(t)$ imply it is a past outer spacelike horizon. In the limit $t \to \infty$ it tends to the lightlike horizon $r = 2m$ (see Fig. 17).

b. The case $4m < t_0 < 8m$

In the situation of Fig. 18, with $t_0 = 6m$, $m = 1$, the horizons are formed at $t_i \simeq 3.30$ with values $\hat{r}_\pm(t_i) = 4.0$ and last forever. In the limit $t \to \infty$, $\hat{r}_+(t)$ tends to $t_0 e^{2t/t_0}$, while $\hat{r}_-(t)$ tends to $2m$.

(1) Along $\hat{r}_+(t)$: The NEC is satisfied for all times and so Theorem I applies. Considering that $q \neq 0$ and $\mathcal{L}_+\Theta_- < 0$ at all times on $\hat{r}_+(t)$ the result is a past outer spacelike horizon.

(2) Along $\hat{r}_-(t)$: The NEC holds at initial times after horizons formation, from $t_i \simeq 3.30$ to $t_c \simeq 3.95$ along this branch of the trapping horizon. Moreover, one has the conditions $q \neq 0$ and $\mathcal{L}_+\Theta_- > 0$ on $\hat{r}_-(t)$, which implies that it is a past outer spacelike horizon (see Fig. 18) in that region. Later than

$t \simeq 3.95$ the NEC is violated and the horizon changes character to timelike, being a past outer horizon in the interval $t \in [t_c, \infty)$. In the limit $t \to \infty$ it asymptotes the lightlike horizon $r = 2m$, a region where the NEC holds also on $\hat{r}_-(t)$.

c. The case $t_0 > 8m$

In the situation of Fig. 19, with $t_0 = 10m$, $m = 1$, the horizons are formed at $t_i = 0.0$ with values $\hat{r}_+(t_i) \simeq 7.2$ and $r_-(t_i) \simeq 2.8$ and last forever. In the limit $t \to \infty$, $\hat{r}_+(t)$ tends to $t_0 e^{2t/t_0}$, while $\hat{r}_-(t)$ tends to $2m$.

(1) Along $\hat{r}_+(t)$: The NEC is satisfied for all times and Theorem I can be applied. The Lie derivative $\mathcal{L}_+\Theta_-$ is positive at initial times but changes to negative values at $t = t_c \simeq 5.93$. Then, $\hat{r}_+(t)$ is a past outer timelike horizon in the interval $t \in [0, t_c]$, and is a past inner spacelike horizon in the region $t \in [t_c, \infty)$.

(2) Along $\hat{r}_-(t)$: The energy conditions are violated. In particular the NEC does not hold along this branch of the trapping horizon and the predictions of the mentioned theorem do not apply here. However, it is

verified that $q \neq 0$ and $\mathcal{L}_+\Theta_- < 0$ all along $\hat{r}_-(t)$ and so it is a past outer timelike horizon.

7. The cases of Sec. V C 4

As commented at the end of Sec. V C 4, these are approximate models that have been implemented to simulate a phase change on the accreting process onto the central object. As a first approximation, we truncated the scale factor in such a way its rate $\dot{a}(t)$ vanishes at very late times. With such a choice, the character of the trapping horizons remains roughly the same as the original models. Moreover, even in these crudely approximated models we used to draw the causal diagrams, the horizon functions $\hat{r}_\pm(t)$ have no jumps with time. The modifications happen just in the limit $t \to \infty$. For instance, in the model of Eq. (58) the only change is in the final value of $\hat{r}_+(t)$ which tends to infinity in the original model, while it approaches a constant (though with a very large value) in the modified model. The energy conditions on it and the chronological character, compatible with Theorem I, do not change. Also, the character of the branch $\hat{r}_-(t)$ remains the same.

---

[1] G. C. McVittie, The mass-particle in an expanding universe, Mon. Not. R. Astron. Soc. **93**, 325 (1933).

[2] A. Einstein and E. G. Straus, The influence of the expansion of space on the gravitation fields surrounding the individual stars, Rev. Mod. Phys. **17**, 120 (1945).

[3] R. C. Tolman, Effect of inhomogeneity on cosmological models, Proc. Natl. Acad. Sci. U.S.A. **20**, 169 (1934).

[4] H. Bondi, Spherically symmetrical models in general relativity, Mon. Not. R. Astron. Soc. **107**, 410 (1947).

[5] T. Biswas and A. Notari, Swiss-cheese inhomogeneous cosmology and the dark energy problem, J. Cosmol. Astropart. Phys. 06 (2008) 021.

[6] V. Marra, E. W. Kolb, S. Matarrese, and A. Riotto, Cosmological observables in a Swiss-cheese universe, Phys. Rev. D **76**, 123004 (2007).

[7] M. Mars, On the uniqueness of the Einstein-Straus model, Classical Quantum Gravity **18**, 3645 (2001).

[8] F. C. Mena, R. Tavakol, and R. Vera, Generalization of the Einstein-Straus model to anisotropic settings, Phys. Rev. D **66**, 044004 (2002).

[9] J. P. Mimoso, M. Le Delliou, and F. C. Mena, Separating expansion from contraction in spherically symmetric models with a perfect fluid: Generalization of the Tolman-Oppenheimer-Volkoff condition and application to models with a cosmological constant, Phys. Rev. D **81**, 123514 (2010).

[10] M. Le Delliou, F. C. Mena, and J. P. Mimoso, Role of shell crossing on the existence and stability of trapped matter

shells in spherical inhomogeneous Λ-CDM models, Phys. Rev. D **83**, 103528 (2011).

[11] M. Le Delliou, J. P. Mimoso, F. C. Mena, M. Fontanini, D. C. Guariento, and E. Abdalla, Separating expansion and collapse in general fluid models with heat flux, Phys. Rev. D **88**, 027301 (2013).

[12] J. P. Mimoso, M. Le Delliou, and F. C. Mena, Local conditions separating expansion from collapse in spherically symmetric models with anisotropic pressures, Phys. Rev. D **88**, 043501 (2013).

[13] A. Maciel, M. Le Delliou, and J. P. Mimoso, Dual null formalism for the collapse of fluids in a cosmological background, Phys. Rev. D **92**, 083525 (2015).

[14] S. N. G. Thakurta, Kerr metric in an expanding universe, Indian J. Phys. B **55**, 304 (1981).

[15] B. C. Nolan, A point mass in an isotropic universe: Existence, uniqueness, and basic properties, Phys. Rev. D **58**, 064006 (1998).

[16] B. C. Nolan, A point mass in an isotropic universe: II. Global properties, Classical Quantum Gravity **16**, 1227 (1999).

[17] B. C. Nolan, A point mass in an isotropic universe: III. The region $R \leq 2m$, Classical Quantum Gravity **16**, 3183 (1999).

[18] N. Kaloper, M. Kleban, and D. Martin, McVittie's legacy: Black holes in an expanding universe, Phys. Rev. D **81**, 104044 (2010).

[19] K. Lake and M. Abdelqader, More on McVittie's legacy: A Schwarzschild–de Sitter black and white hole embedded

in an asymptotically ΛCDM cosmology, Phys. Rev. D **84,** 044045 (2011).

[20] A. M. da Silva, M. Fontanini, and D. C. Guariento, How the expansion of the Universe determines the causal structure of McVittie spacetimes, Phys. Rev. D **87,** 064030 (2013).

[21] A. Maciel, D. C. Guariento, and C. Molina, Cosmological black holes and white holes with time-dependent mass, Phys. Rev. D **91,** 084043 (2015).

[22] S. A. Hayward, General laws of black-hole dynamics, Phys. Rev. D **49,** 6467 (1994).

[23] S. A. Hayward, Quasilocal gravitational energy, Phys. Rev. D **49,** 831 (1994).

[24] S. A. Hayward, Gravitational energy in spherical symmetry, Phys. Rev. D **53,** 1938 (1996).

[25] S. A. Hayward, Unified first law of black-hole dynamics and relativistic thermodynamics, Classical Quantum Gravity **15,** 3147 (1998).

[26] M. Mars and J. M. Senovilla, Trapped surfaces and symmetries, Classical Quantum Gravity **20,** L293 (2003).

[27] J. M. Senovilla, Trapped surfaces, Int. J. Mod. Phys. D **20,** 2139 (2011).

[28] D. C. Guariento, M. Fontanini, A. M. da Silva, and E. Abdalla, Realistic fluids as source for dynamically accreting black holes in a cosmological background, Phys. Rev. D **86,** 124020 (2012).

[29] V. Faraoni, Analysis of the Sultana-Dyer cosmological black hole solution of the Einstein equations, Phys. Rev. D **80,** 044013 (2009).

[30] V. Faraoni, C. Gao, X. Chen, and Y.-G. Shen, What is the fate of a black hole embedded in an expanding universe? Phys. Lett. B **671,** 7 (2009).

[31] J. Sultana and C. C. Dyer, Cosmological black holes: A black hole in the Einstein-de Sitter universe, Gen. Relativ. Gravit. **37** 1347 (2005).

[32] M. Carrera and D. Giulini, Generalization of McVittie's model for an inhomogeneity in a cosmological spacetime, Phys. Rev. D **81,** 043521 (2010).

[33] B. R. Majhi, Thermodynamics of Sultana-Dyer black hole, J. Cosmol. Astropart. Phys. 05 (2014) 014.

[34] H. Culetu, On the time dependent Schwarzschild–de Sitter spacetime, J. Phys. Conf. Ser. **437,** 012005 (2013).

[35] C. A. Kolassis, N. O. Santos, and D. Tsoubelis, Energy conditions for an imperfect fluid, Classical Quantum Gravity **5,** 1329 (1988).

[36] M. Carrera and D. Giulini, Influence of global cosmological expansion on local dynamics and kinematics, Rev. Mod. Phys. **82,** 169 (2010).

[37] R. M. Wald, *General Relativity* (University of Chicago Press, Chicago, 1984).

[38] S. W. Hawking and G. F. R. Ellis, *The Large Scale Structure of Space-Time* (Cambridge University Press, Cambridge, 1973).

[39] L. Andersson, M. Mars, and W. Simon, Local Existence of Dynamical and Trapping Horizons, Phys. Rev. Lett. **95,** 111102 (2005).

[40] P. H. Chavanis, Cosmology with a stiff matter era, Phys. Rev. D **92,** 103004 (2015).

[41] P. S. Letelier, String cosmologies, Phys. Rev. D **28,** 2414 (1983).

[42] A. Vilenkin, String Dominated Universe, Phys. Rev. Lett. **53,** 1016 (1984).

[43] R. H. Price, In an expanding universe, what doesn't expand?, arXiv:gr-qc/0508052.